Dissecting the roles of tight junction membrane proteins in mechanical resistance of apical junctions

Nguyen, Thanh Phuong

Department of Physiological Sciences
School of Life Science
The Graduate University for Advanced Studies, SOKENDAI

30th June 2023

Contents

Abbreviations

TJ	Tight junction
AJ	Adherens junction
JAM	Junctional Adherens Molecule
EM	Electron microscopy
DL1	Distal Loop 1
CAR	Coxsackie and Adenovirus Receptor
MARVEL	MAL and related proteins for vesicle trafficking and membrane link
TAMPs	TJ-associated MARVEL proteins
TEER	Transepithelial electrical resistance
MDCK II	Madin-Darby canine kidney II
KO	Knock out
ZO-1	Zonula occludens -1
GFP	Green fluorescent protein
STED	Stimulated Emission Depletion
MHCIIA	Myosin heavy chain IIA
MHCIIB	Myosin heavy chain IIB
ROCK	Rho-associated Protein Kinase
LIMK	LIM Kinase
HA	Haemagglutinin
PFA	Paraformaldehyde
TCA	Trichloroacetic acid
RT	Room temperature
DMEM	Dulbecco's Modified Eagle Medium
FBS	Fetal bovine serum
EDTA	Ethylenediaminetetraacetic acid
PBS	Phosphate buffered saline
DMSO	Dimethyl sulfoxide
PCR	Polymerase chain reaction
SDS-PAGE	Sodium dodecyl-sulfate polyacrylamide gel electrophoresis
DTT	Dithiothreitol
TBS	TRIS-buffered saline
BSA	Bovine serum albumin

Summary

Epithelia cover the outer surface of our body and the inner surface of internal compartments. Epithelia serve as a barrier to protect the entire body from the external environment. Epithelia are constantly exposed to mechanical stress, internally and externally. Thus, epithelial cells must resist that stress to preserve tissue integrity, by forming intercellular junctions, including tight junctions (TJs), adherens junctions (AJs), and desmosomes. TJs and AJs together are often called "apical junctions". Among them, it is widely accepted that AJs are critical for tension regulation via mechanical coupling with actin cytoskeleton, and desmosomes provide strong cell-cell adhesion across cells via linkage to intermediate filaments. Unlike those, the specific impact of TJs on mechanical resistance has remained unclear for a long time, due to technical limitations to specifically and completely perturb TJs. Our group has recently established the epithelial Madin-Darby canine kidney (MDCK) II cell lines that specifically and completely disrupt TJ structure and function, making the cells a decent model to analyze how TJs depletion causes subsequent defects in epithelial integrity. By utilizing this model system, I investigated whether and to what degree TJ proteins contribute to epithelial integrity against mechanical stress.

Here I report that spontaneous breakages of apical junctions were observed in epithelial MDCK II cells depleted of two types of TJs-associated integral membrane proteins claudin and JAM-A (claudins/JAM-A KO cells), which lack entire TJs. Cell-cell junction morphology was visualized by apical junction marker ZO-1, which showed sharp and continuous staining at the apical region of cell-cell contacts in control MDCK II cells. In contrast, ZO-1 staining in claudins/JAM-A KO cells displayed peculiar discontinuous staining at apical junctions, and large ZO-1 gaps were occasionally seen, suggesting that apical junction integrity was disrupted.

To investigate how these junction breakages arose in claudins/JAM-A KO cells, I examined apical junction dynamics in claudins/JAM-A KO cells to compare with that in MDCK II cells. Live-cell imaging revealed that junction breakages, marked by the loss of GFP-tagged ZO-1, occurred concomitantly with the loosening of circumferential actin bundles, suggesting a strong spatial-temporal correlation between junction breakages and actomyosin disorganization. I further investigated whether actomyosin plays a causal role in junction breakages in claudins/JAM-A KO cells, and observed that pharmacological perturbation of actin polymerization indeed enhances the junction breakage phenotype, pointing out that actin cytoskeleton plays critical roles in the apical junction integrity dependent on claudin and JAM-A.

Structure-function analysis of claudin and JAM-A suggested that they preserve apical junction integrity in two pathways. First, claudin and JAM-A form trans-interactions across cells

most likely to physically strengthen apical junctions. Second, claudin and JAM-A mechanically couple apical junctions to actin cytoskeleton via TJ-associated cytoplasmic scaffolding protein ZO-1. These results suggested the mechanical coupling between neighboring cells through claudin and JAM-A. I next focused on ZO-1, an intermediate linker connecting claudin and JAM-A to actin cytoskeleton. Super-resolution stimulated emission depletion imaging to evaluate the conformational change of ZO-1 showed that in the presence of claudin and JAM-A, ZO-1 molecules were oriented with the N-terminus toward the plasma membrane and the C-terminus toward the cytoplasm, and ZO1 undergoes a conformational change to unfold its structure. In contrast, although ZO-1 molecules in claudins/JAM-A KO cells showed similar orientation to those in MDCK II cells, the distance between the N-terminus and C-terminus of ZO-1 was shortened, indicating that ZO-1 prefers "less-stretched" conformation. This suggests that claudin and JAM-A support apical junction integrity by regulating the conformational change of ZO-1.

Further depletion of another IgG-like domain-containing adhesion molecule CAR in claudins/JAM-A KO cells exaggerated the junction breakages phenotype, with various large ZO-1 gaps observed. Claudins/JAM-A/CAR KO cells also displayed more random orientation of ZO-1, with N-terminus no longer exclusively localized to membrane-proximal regions but were also found at the membrane-distal regions facing inward the cytoplasm. This indicates that CAR, together with claudin and JAM-A, supports the apical junction integrity and regulates the nanometer-scale ordering of ZO-1.

In conclusion, my study demonstrated that TJ membrane proteins, including claudin, JAM-A, and CAR, coordinately regulate the mechanical resistance of apical junctions in epithelial cells.

Introduction

Molecular structure of tight junctions

Epithelia line the body surface and organ cavities, serving as barriers between internal and external environments. The most basic form of the epithelia is the simple epithelium, in which a monolayer of cells tightly adheres to one another via intercellular junctions, namely "junctional complexes" (Farquhar and Palade, 1963). Junctional complexes include tight junctions (TJs), adherence junctions (AJs), and desmosomes (**Figure 1**), among which TJs and AJs are collectively referred to as "apical junctions". On ultrathin sections, TJs are found at the most apical part of cell-cell contacts, where two plasma membranes tightly adhere to each other (**Figure 3**; left panel; arrow), thereby completely sealing the paracellular space (Farquhar and Palade, 1963; Anderson and Van Itallie, 2009; Shen et al., 2011; Zihni et al., 2016). On free-fracture replica EM, TJs are visible as an anastomosing strand network (TJ strands) (Staehelin LA., 1973).

TJs are composed of different types of integral membrane proteins, including claudin family proteins, tight junction-associated MARVEL proteins (TAMPs), and immunoglobulin superfamily proteins. Claudin has an N-terminal cytoplasmic domain, four transmembrane domains, two extracellular loops, a short cytoplasmic turn, and a C-terminal cytoplasmic domain, which contains a PDZ domain binding motif (Furuse et al., 1998; Günzel and Yu, 2013). Claudin establishes the backbone of TJ strands, forming "head-to-head" trans-interactions across neighboring cells (Furuse et al., 1998; Morita K. et al., 1999; Suzuki et al., 2014). Besides claudin, occludin is another TAMPs, a tetra-span transmembrane protein that shares similar membrane-spanning topology with claudin. When occludin was exogenously expressed in mouse L fibroblasts (L cells), it assembled in cell-cell contacts from both neighboring cells, suggesting trans-interaction of occludin (Furuse et al., 1998). Although detailed roles of TAMPs

in TJ formation have remained unclear, a recent study showed that occludin and tricellulin collectively facilitate the formation of anastomosing TJ strand networks to regulate epithelial barrier function (Saito et al., 2021). TJ-associated immunoglobulin superfamily proteins contain junction adhesion molecules-A (JAM-A), and coxsackie and adenovirus receptor (CAR). JAM-A is a single-span transmembrane protein that contains two extracellular Ig-like domains, a transmembrane domain, and a C-terminal cytoplasmic domain carrying a PDZ domain binding motif (Martin-Padura et al., 1998; Prota AE., 2003). The most distal domain of JAM-A, so-called distal loop 1, was found to be responsible for both cis-interaction of JAM-A molecules from the same cell surface and trans-interaction of JAM-A molecules across neighboring cells (Kostrewa D. et al., 2001; Prota AE., 2003; Mandell et al., 2004; Monteiro et al., 2014). CAR was first identified as a receptor for adenovirus and coxsackievirus (Bergelson et al., 1997), and later shown to be colocalized with ZO-1 at TJs (Cohen et al., 2001). Although CAR was reported to have potential roles in epithelial permeability and homeostasis (Raschperger et al., 2006; Carolyn B. Coyne & Jeffrey M. Bergelson., 2005), its biological importance in TJs has largely remained to be determined.

Many TJ-associated integral membrane proteins are known to bind to ZO-1, a TJ-associated cytoplasmic scaffolding protein. ZO-1 is a member of the ZO family, including ZO-1, ZO-2, and ZO-3. ZO-1 consists of three PDZ domains, an SH3 domain, and a GUK domain from their N-termini (Stevenson et al., 1986; Gumbiner et al., 1991; Itoh et al., 1993). Claudin and JAM-A bind to PDZ-1 and PDZ-3 domains of ZO-1, respectively, via their C-terminal PDZ domain binding motives (Itoh et al., 1999; Bazzoni et al., 2000; Ebnet et al., 2000; Itoh et al., 2001). Meanwhile, the C-terminal cytoplasmic domain of occludin binds to the SH3-GUK region of ZO-1 (Tash et al., 2012). CAR was reported to be co-precipitated with ZO-1 in cell lysate, although the detailed interacting domains have not yet been clarified (Cohen et al., 2001). Importantly, the C-terminal half of ZO-1 contains an F-actin-binding domain, suggesting the role

of ZO-1 in the linkage between TJ membrane and actin cytoskeleton (Fanning et al., 1998; Fanning et al., 2002; Belardi et al., 2020) (**Figure 2**).

Mechanical stress resistance in epithelia

Epithelia are constantly exposed to intrinsic and extrinsic mechanical stress. This stress can cause a rupture force to shear epithelial cells apart and disrupt the intact epithelium. To preserve epithelial integrity, cells withstand mechanical stress by forming intercellular junctions, including TJs, AJs, and desmosomes (Farquhar and Palade, 1963). Intercellular junctions are well known to play critical roles in mechanical stress resistance: AJs sense and transduce mechanical force from the cell membrane through the cadherin/catenin complex to the actin cytoskeleton, thus regulating the intercellular tension (Matsunaga et al., 1988; Takeichi, 1991; Kintner, 1992; Harris et al., 2012). Desmosomes are specialized for providing hyper-adhesive strength by connecting membrane contacts to intermediate filaments network; desmosome malfunction disrupts epithelial tissue integrity and causes pathological symptoms of skin blistering, known as pemphigus (Amagai et al., 1991). In contrast to AJs and desmosomes, little is known about the role of TJs in the mechanical resistance of epithelial cell junctions. A recent study reported that ZO-1 functions as a TJ-specific force sensor molecule (Spadaro et al., 2017). Using molecular fluorescent probing in conjunction with advanced super-resolution imaging, they discovered that ZO-1 changes its molecular conformation from the folded structure to the stretched structure in response to tension. Later, Hass and colleagues investigated the mechanosensitive properties of ZO-1 and found that ZO-1 can bear tension loaded on its molecule, which can be regulated by either extracellular matrix stiffness or JAM-A (Haas et al., 2020). These findings together suggest a possible role of TJs in mechanosensation in epithelial cells.

Cell model to distinctively examine the roles of TJs in mechanical resistance

Our earlier work on MDCK II cells showed that simultaneous removal of claudin-1, -2, -3, -4, and -7 results in the complete loss of claudin-based TJ strands (claudins KO cells) (Otani et al., 2019). Epithelial integrity was compromised in claudins KO cells: transepithelial electrical resistance (TEER) was reduced, and paracellular diffusion of small solutes such as fluorescein remarkably increased. However, claudin KO cells still maintained close plasma membrane appositions at the most apical part of cell-cell contacts (**Figure 3**; middle panel; white arrow) and restricted paracellular diffusion of macromolecules. When JAM-A was further removed from claudins KO cells to establish claudins/JAM-A KO cells, they displayed more severely compromised epithelial integrity, with enlarged intercellular space at apical junctions (**Figure 3**; right panel; white arrow), and loss of the paracellular diffusion barrier to macromolecules (Otani et al., 2019). The establishment of claudins/JAM-A KO cells, which completely and specifically lack TJ structure and function, provided a decent model to distinctively examine the roles of TJs in mechanical resistance.

In this study, I investigate the mechanism underlying claudins/JAM-A KO cells lacking TJs exhibit focal apical junction breakages upon mechanical stress. I show that multiple TJ-associated integral membrane molecules, including claudin, JAM-A, and CAR collaborate to maintain the integrity of epithelial cell-cell junctions and the ZO-1 conformational change, which strongly correlates with the ability of apical junctions to resist mechanical stress. All results together point to the importance of TJ proteins in the mechanical resistance of apical junctions in epithelia.

Materials and methods

Cell culture

Mardin-Darby canine kidney (MDCK) II cells (Richardson et al, 1981) and mouse fibroblast (L cells) were used in this study. Cells were maintained in low glucose Dulbecco's Modified Eagle Medium (DMEM) (Nissui; #05919) supplemented with 2mM L-glutamine (Nacalai Tesque; # 16948) and 10% Fetal bovine serum (FBS) (Bio-West; #S1820-500) at 37°C, 5%CO_2. Media were changed every 2-3 days. Cells were passed every 6-8 days using 0.25% crude trypsin in 1mM Ethylenediaminetetraacetic acid (EDTA) in Ca^{2+} - Mg^{2+} free phosphate-buffered saline (1xPBS). Cells maintained in culture media up to a maximum of 8 passages (two months) were used for experiments. The establishment of claudins/JAM-A KO cells that were generated from MDCK II cells has been described previously (Otani et al., 2019).

For experiments using MDCK II cells, cells used for immunocytochemistry were prepared as follows: $3x10^5$ cells were seeded on a 12-well trans-well filter (12mm diameter; 0.4μm pore size; Corning; #3401) and cultured for 5-7 days. For immunocytochemistry analysis using L cells: $3x10^5$ cells on 6-well plates containing coverslips. After 48 hours, coverslips were collected and subjected to immunostaining. Cell preparation for transfection is as same as in MDCK II cells.

For live-cell imaging, $1x10^5$ cells were placed at the center of the Iwaki glass dish (27mm diameter; #3910-035) or Matek glass dish. Cells were cultured in low glucose DMEM (Nacalai Tesque; #08490-05) supplemented with 10% FBS and Pen Strep Glutamine (Gibco; #10378-016). For actomyosin perturbation analysis, $3x10^5$ cells cultured in a 12-well trans-well filter plate for 48 hours (for subsequent immunocytochemistry analysis) were used for drug treatments.

Antibodies

The following primary antibodies were used for immunocytochemistry and western blotting analyses in this study: mouse anti-ZO-1 (T8754), rat ZO-1 (R26.4C), rabbit anti-ZO-1 (Thermo Fisher Scientific; #61-7300), rabbit anti-ZO-2 (Thermo Fisher Scientific; #38-9100), rabbit anti-claudin-1 (Thermo Fisher Scientific; #51-9000), rabbit polyclonal anti-human JAM-A (Invitrogen; #PA5-120157), rat anti-occludin (MOc37; Saitou et al, 1997)), rat anti-E-cadherin (clone ECCD-2; Takara; #M108; Shirayoshi, 1986), rabbit anti-1/s-afadin (Sigma-Aldrich; #A0224), rabbit anti-α-catenin (Sigma-Aldrich; #C2081), rat anti-α-18 (Nagafuchi and Tsukita, 1994), mouse anti-vinculin (clone VIN-11-5; #V4505; Sigma-Aldrich), rabbit anti-Myosin heavy chain IIA (MHCIIA) (Sigma-Aldrich; #M8064), rabbit anti-Myosin heavy chain IIB (MHCIIB) (BioLegend; #909901), rat anti-HA (clone 3F10; Roche), mouse anti-FLAG (Wako; #014-22383), rabbit polyclonal anti-CAR (kindly provided by Jeffrey M. Bergelson), mouse monoclonal anti-α-tubulin (clone DM1A; Invitrogen; #14-4502-82).

The following secondary antibodies were used for immunohistochemistry: Alexa Fluor 488 donkey anti-mouse IgG (Molecular Probes; #A21202), Alexa Fluor 488 donkey anti-rabbit IgG (Molecular Probes; #A21206), Alexa Fluor 488 donkey anti-rat IgG (Molecular Probes; #A21208), Alexa Fluor™ 555 donkey anti-mouse IgG (Invitrogen; #A31570), Alexa Fluor™ 555 donkey anti-rabbit IgG (Invitrogen; #A31572), Alexa Fluor™ 555 goat anti-rat IgG (Invitrogen; #A21434), Alexa Fluor 647-conjugated Phalloidin (Invitrogen; #A22287), sheep anti-mouse IgG HRP-conjugated whole antibody (GE Healthcare; #NA931V); donkey anti-rabbit HRP-conjugated F(a'b')2 fragment (GE Healthcare; #NA9340V).

Expression vectors

ZO1-GFP expression vectors (pCANw-mZO1-GFP and pCAH-dZO1-GFP) were produced as follows: fragment encoding GFP tag was PCR-amplified from vector pEGFP-N3 and inserted into the C-termini of a full-length mouse or dog ZO1. The ZO1-GFP fragments were

subsequently ligated into pCANw vectors using Infusion ligation reagent (Takara Bio) following manufacture instructions. For two-color live-cell imaging constructs: the expression vector of Lifeact7-mCherry was made by subcloned Lifeact7-mCherry fragment (addgene; #54491) into pCAB vector.

For reconstituting claudin-1 or JAM-A mutants in claudins/JAM-A KO cells: expression vectors encoding full-length claudin-1 or JAM-A were produced by cloning DNA fragments encoding mouse claudin-1 or human JAM-A into pCANw vector to generate pCANw-claudin-1 and pCANw-JAM-A, respectively. The pCAN-claudin-1 vector was subsequently used as the frame to generate trans-interaction deficient mutant claudin-1[F147A] (substitution of an amino acid Phenylalanine-147th to Alanine) and ZO1 binding deficient mutant claudin-1[ΔYV] (deletion of amino acid Tyrosine-211th and Valine-212th). Similarly, pCANw-JAM-A was used to generate trans-interaction deficient mutant JAM-A[ΔDL1] (deletion of entire DL1 domain containing acid amin 28th ->125th) and ZO-1 binding deficient mutant JAM-A[ΔLV] (deletion of amino acid Leucine-298th and Valine-299th). Mutations were generated using the site-directed mutagenesis method.

For checking ZO-1 conformational status: HA tag (YPYDVPDYA)and FLAG tag (YKDDDDK) were inserted into the primers used to PCR-amplify full-length dog ZO-1 fragment. The PCR-amplified HA-dZO1-Flag fragment was subsequently cloned into pCANw vector using Infusion.

All constructs were finally checked by the Sanger sequencing method.

Transfection

All cells used for transfections were in the second passage of cell culture. In general, for stable transfection of MDCK II or L cells: 3x10^5 cells were seeded on 6-well plates one day prior to transfection. On the day of transfection, 5µg of plasmid constructs (for the large constructs of ZO1-GFP and HA-dZO1-Flag) or 2,5µg (for other constructs) was diluted in 200µL opti-MEM

(Gibco; #31985-070), mixed well with Plus reagent and Lipofectamine LTX at the ratio of 1:1:1,5. The mixture was left untouched at room temperature for 30 minutes before being added to the cell culture. After six hours of incubation at 37°C, 5%CO_2, the medium was changed. On the second day, cells were harvested and passed to 10-cm plates at limited dilution to allow colony formation. From the third day, selective antibiotics of either 500mg/mL G418 (stock 50mg/mL; #16513-26; Nacalai tesque); or 200µg/mL Hygromycin B (stock 50mg/mL; #09287-84; Nacalai tesque) or 2µg/mL Blascitidin (stock 10µg/L) were added to the cell culture. The medium was changed every three days up to the following two weeks. Multiple surviving clones were picked and checked by immunocytochemistry and western blotting analysis. The three best clones per cell line were selected for freeze-stock or maintenance in a DMEM supplied with antibiotics.

Protocol for transient transfection of MDCK II or fibroblast L cells was the same as stable transfection, except after adding DNA-Lipofectamine LTX mixture into cell culture, the cells were incubated at 37°C, 5%CO_2 for 48 hours straight without media change and no added selective antibiotics. After 48 hours, cells were directly subjected to further analysis.

Immunocytochemistry

Cells cultured on trans-well plates or coverslips were fixed with 1-2% paraformaldehyde (PFA) (room temperature (RT),15 minutes), 10% trichloroacetic acid (TCA) (4°C, 15 minutes), or 100% Methanol (RT, 10 minutes). Fixation of 1%PFA was used for E-cadherin, afadin, α-catenin, α-18, vinculin, HA, and Flag. Fixation of 2%PFA was used for ZO-1, F-actin, Myosin IIA, Myosin IIB, and CAR. Fixation of 10%TCA was used for ZO-2. Fixation of 100% methanol was used for claudin-1 and occludin. After fixation, cells were washed three times with 1x phosphate buffer saline (PBS), permeabilized with 0.1% TritonX-100 in PBS (15 mins, RT), rinsed once with 1xPBS, and blocked with 10% FBS (RT, 30 minutes). Filters were cut in half and probed with primary antibodies diluted in a blocking solution (1 hour, RT). Cells were then

washed three times with 1xPBS and probed with secondary antibodies diluted in a blocking solution (1 hour, RT, avoid light). Finally, cells were washed three times with 1xPBS and mounted using FluoroSave Reagent (Calbiochem®; #345789). For the preparation of fixed samples used for Stimulated emission depletion (STED) imaging, samples were mounted using ProLong™ Diamond Antifade Mountant (Invitrogen; P36961; 20uL).

Western blotting

Cells grown on 35 mm dishes were rinsed once with ice-cold 1xPBS and were lysed with 200 µL of Laemmli sample buffer supplemented with 100 mM Dithiothreitol (DTT), sonicated, and boiled at 97°C for 5 min. Samples were separated by Sodium dodecyl-sulfate polyacrylamide gel electrophoresis (SDS-PAGE) using standard methods, and a 20 µl sample was loaded per lane. The separated proteins were transferred to 0.45 mm pore Protran nitrocellulose transfer membranes (Whatman, #10-401-196). Membranes were blocked with 5% skim milk or 3% Bovine serum albumin (BSA) dissolved in 0.1% Tween-20 in TRIS-buffered saline (TBS) for 1 h at RT. Primary antibodies were diluted in the blocking solution and incubated with the membrane overnight (4°C, shaking). The next day, membranes were rinsed three times with 0.1% Tween-20 in TBS and subsequently incubated with the secondary antibodies diluted in the blocking solution for 1 h at RT. After three washes with 0.1% Tween-20 in TBS, signals were detected by chemiluminescence using ECL Prime Western Blotting Detection Reagents (Cytiva; #RPN2232). Images were obtained using LAS3000 mini (Fujifilm), and data were processed and analyzed using Fiji/ImageJ 1.53t software.

Confocal imaging

Confocal images were obtained using NIKON AX-R confocal laser scanning microscope system mounted on Eclipse Ti2 inverted microscope, with objective lens CFI PLAN Apochromat

Lambda D 60x Oil (NA 1.42) and diode lasers 488/561/640 nm. Images were achieved using NIS-Element C Imaging software (from Nikon Solutions).

For STED imaging, cells were imaged using a TCS SP8 STED confocal system (Leica microsystems, Germany) mounted on a DMI8 inverted microscope, using an objective lens HC PL APO CS2 100x Oil (NA 1.4) with confocal diode laser 488/555nm and STED diode laser 592/660nm. Image acquisition was achieved using Leica Application Suite X software.

Live-cell imaging

Live-cell imaging of MDCK II and claudins/JAM-A KO cells expressing exogenous ZO1-GFP was performed as followed: $1x10^5$ cells seeded on Iwaki glass-bottom dish (Iwaki; #3910-035) was cultured in phenol red-free DMEM, low glucose (Nacalai Tesque; #08490-05), supplemented with 10% FBS and Penicillin-Strepomycin-Glutamine (Gibco; #10378-016). Cells were imaged on Yokogawa & Olympus CellVoyager VC1000 confocal scanner system equipped with dual Nipkow disks- EMCCD camera (Hamamatsu) and an environmental control chamber, using an objective lens 40x Dry (NA 1.3) with diode laser 488nm. Cell recording started from the time cells attached to the dish bottom and stopped when the cells reached fully confluent (5 days). Cells were imaged with an interval time of 12 minutes, the confocal z-stack setting was 22µm focus range and 1µm z-step size. Movie acquisition was done using Yokogawa CV1000 software and later analyzed using Fiji/ImageJ 1.53t software.

For two-color live-cell imaging of claudins/JAM-A KO cells co-expressing exogenous ZO1-GFP and Lifeact7-mCherry, $1x10^5$ cells seeded on Iwaki glass-bottom dish on the second day were imaged using Yokogawa & Olympus CellVoyager CV1000 confocal scanner system using an objective lens 60x Silicone (NA 1.35) with diode laser 488nm and 561nm. Cells were imaged with 1 minute interval time, the confocal z-stack setting was 20µm focus range and 0,6µm z-step size. Movie recording was performed for 10 hours straight with cells growing in

sub-confluent conditions. Time-lapse movie acquisition was obtained using Yokogawa CV1000 software and proceeded using Fiji/ImageJ 1.53t software.

Actomyosin perturbation assay

The following reagents were used: Rho-associated Protein Kinase (ROCK) inhibitor Y-27632 (Wako; #030-24021; 10µM), blebbistatin (Wako; #021-17041; 100µM), LIM kinase (LIMK) inhibitor BMS-5 (Selleckchem; 10µM), latrunculin A (Sigma-Aldrich; #428-021; 0,3µM). H_2O was used as a vehicle for Y-27632, and DMSO was used as a vehicle for others. In brief, cell culture media were replaced with pre-warmed DMEM containing drugs at the indicated concentration and incubated for 1 hour (Latrunculin A) or 3 hours (for others) at 37°C, 5%CO_2. Cells were then subjected to immunocytochemistry.

Quantification and statistics

Images were processed using Fiji/ImageJ 1.53t software (National Institutes of Health). Specifically, junction breakages were quantified as follows: (1) Images were denoised using the band-pass filter to filter out the small structures up to 3 pixels and large structures up to 40 pixels; followed by the median filter (1-2 pixels); (2) segmentation to remove outliers was done by threshold (standard), followed by binarization and skeletonization; (3) break-end points were extracted by averaging filter, following by threshold (Otsu) and band-pass filter; (4) the outliners < 1pixel were removed from images; (5) the number of junction endpoints was counted by "analyze particles" function of ImageJ; (6) number of junction endpoints was finally normalized to the observed area (294 µm x294µm) to obtain the number junction endpoints per unit area.

Cell stretching degree was determined by measuring the cell circumference of interest. The starting point of cell stretching degree was specified as L_o, and L was defined as the maximum change in cell circumference upon maximal stretching. The degree of stretching was measured as ($\Delta L/ L_o$) x100 (%). Meanwhile, ZO1-GFP intensity was measured by measuring average

intensity along the cell circumference. Initial intensity I_o is the ZO1-GFP intensity at the starting point of stretching (L_o), while "I" is the ZO1-GFP intensity when the cell reaches maximum stretching (L). Change in ZO1-GFP was measured as $(\Delta I/ I_o)$ x100 (%).

To measure the distance between N-terminus HA tag and C-terminus FLAG tag of ZO-1, a line-scan was drawn across each pair of HA/FLAG puncta to obtain a fluorescent intensity profile, and the distance between two fluorescent peaks was measured. Only pairs that seem to be doublets were counted. The order parameter was quantified as follows: (1) measure the angle between the N-terminus and C-terminus of ZO-1; (2) mean angle of particles within a single image was established and used to calculate the variation of individual vectors from the average vector; (3) order parameter was determined using previously validated formula $S = (3\cos2-1)/2$ (Doi, Masao; Soft Matter Physics; 2013; *Oxford Academic*).

Excel (Microsoft) was used for statistical type 1 ANOVA followed by the Tukey test and to generate graphs.

Results

Apical junction integrity defects observed in claudins/JAM-A KO cells

I first compared the morphology of apical junctions in claudins/JAM-A KO cells with that of control MDCK II cells by immunofluorescent staining of ZO-1. In MDCK II cells, ZO-1 localized at apical cell-cell contacts sharply and showed a honeycomb pattern (Figure 4A). In contrast, the ZO-1 signal in claudins/JAM-A KO cells showed occasional discontinuity at apical junctions, suggesting that the integrity of apical junctions was disrupted (Figure 4A'-2; arrow). A large ZO-1 gap was seen in a severe case (Figure 4A'-1; asterisk). As claudins/JAM-A KO cells lack the TJ structure completely, ZO-1 was likely to localize at AJs. I named this phenomenon "junction breakage" and quantified its frequency (Figure 4B).

Further characterization of other TJ proteins (occludin and ZO-2) and AJ proteins' (afadin and E-cadherin) distribution by immunofluorescence staining revealed that all these proteins showed discontinuous staining at apical junctions in claudins/JAM-A KO cells (Figure 5, A-D"). Nevertheless, puncta-signals of E-cadherin appeared normal, (Figure 5, E-E'', white arrow), indicating lateral cell-cell contacts in claudins/JAM-A KO cells. Taken together, these observations indicate that claudins and JAM-A are required for apical junction integrity.

Mechanical stretching provoked junction breakages

To elucidate the mechanism of junction breakages, I investigated the dynamics of apical junctions in claudins/JAM-A KO cells. I established MDCK II and claudins/JAM-A KO cells stably expressing exogenous ZO-1 tagged with GFP (ZO1-GFP) and performed live-cell imaging. Time-lapse movies revealed that ZO1-GFP signals in MDCK II cells were maintained continuously when the cells underwent stretching and shrinking (Figure 6A) or during cell division (Figure 6B). Meanwhile, in claudins/JAM-A KO cells, junctional breakages occurred when the cells underwent spontaneous stretching (Figure 6C). Junction breakages were also

observed in dividing cells and the neighboring cells (Figure 6D). Of note, junction breakages in stretched cells or daughter cells after mitosis were eventually repaired, suggesting that the junction breakage is a temporary defect of apical junctions. Consistently, claudins/JAM-A KO cells exhibited a dramatic decrease in the intensity of ZO1-GFP signals correlated with the increase in cell circumference upon stretching, while MDCK II cells did not (Figure 6E, F). Quantitative image analysis of the change in cell circumference indicated cell stretching degree and the intensity of ZO-1-GFP signals indicated junction strength revealed that claudin/JAM-A KO cells underwent junction breakages above a certain threshold of stretching (~30% stretching), while MDCK II cells withstood the similar stretching degree (Figure 6G). Taken together, my data indicate that claudin and JAM-A regulate apical junction integrity upon mechanical stretching.

Actomyosin disorganization was observed at junction breakages

I next focused on actomyosin, the major force-generating system of the cell. I visualized the actomyosin network by super-resolution Stimulated Emission Depletion (STED) imaging of immunofluorescence staining. In MDCK II cells, F-actin, Myosin IIA, and Myosin IIB were mostly localized in the cytoplasm and only weakly detected at apical junctions (data not shown). In contrast, claudins/JAM-A KO cells displayed linear and thick actomyosin distribution along intact apical junctions (Figure 7, A, B-1, E, F-4, I, J-7). At junction breakages, the loss of ZO1 was accompanied by disorganization of actomyosin: the circumferential actomyosin bundles were loose or detached into two separated lines (Figure 7, A, B-2, E, F-5, I, J-8.). Of note, actomyosin bundle again incorporated into junctional area where ZO-1 was still persisted (C, D-3; G, H-6; K, L-9).

The thick actomyosin staining observed in claudins/JAM-A KO cells suggested a possibility of elevated intercellular tension. The intercellular tension is known to be sensed and transduced through E-cadherin-based AJs to the circumferential actomyosin through α/β-catenin

complex (Yonemura et al., 2010). In response to elevated intercellular tension, α-catenin undergoes a conformational change from a "folded" to a "stretched" structure. "Stretched" α-catenin exposes the binding site for α-18 and vinculin, subsequently recruiting these proteins to junction area (Yonemura et al., 2010; Kim T.J et al.,2015; Bertocchi, C et al.,2017). I compared the intercellular tension between MDCK II cells and claudins/JAM-A KO cells by examining immunofluorescence staining of α-18 and vinculin. The vinculin and α-18 signal was barely visible in MDCK II cells, whereas they accumulated at apical junctions in claudins/JAM-A KO cells (Figure 8, A-D''). There was no detectable difference in total α-catenin staining between control and KO cells (Figure 8, A', B'). These observations indicate that intercellular tension is elevated along apical junctions in claudins/JAM-A KO cells.

Since the disorganization of actomyosin was strongly coupled with junction breakages, I next examined the spatial-temporal relationship between actin dynamics and junction breakages. I established claudins/JAM-A KO cells stably expressing an apical junction marker ZO1-GFP and F-actin marker Lifeact7-mCherry. The cells were then used for two-color live-cell imaging at a sub-confluent condition, in which the chance of junctional breakages increased because of active F-actin dynamics. Time-lapse movies revealed that junction breakages occurred concomitantly with the loosening of circumferential F-actin bundles (Figure 9, A-B), suggesting a strong correlation between the junction breakage and actomyosin disorganization. Upon the repair of broken apical junctions, the re-assembly of actin bundles preceded the junctional re-localization of ZO1-GFP (Figure 9, C-F; yellow and red arrow). Altogether, these data suggest that actomyosin organization is critical for apical junction integrity in claudins/JAM-A KO cells under mechanical stress.

Actin polymerization is essential for apical junction integrity in claudins/JAM-A KO cells

As actomyosin organization was strongly correlated with junction breakages in claudins/JAM-A KO cells, I investigated the role of actomyosin in the integrity of apical junctions by pharmacologically disturbing actomyosin organization and evaluate junction integrity via ZO-1 immunostaining. RhoA signaling has been known to play essential roles in regulating actomyosin organization (Ridley A.J et al., 1992; Hall A., 1998; Burridge, K., & Wennerberg, K., 2004). RhoA signaling occurs through a protein kinase cascade where RhoA first binds to and activate Rho-associated protein kinase (ROCK). Activated ROCK in turn elevates myosin light chain phosphorylation and subsequently promotes myosin contractility (Amano M. et al., 1996; Kimura et al., 1996; Chrzanowska-Wodnicka, M., & Burridge, K., 1996). My data showed that inhibition of ROCK activity by Y-27632 (Ishizaki T. et al., 2000) had no effect on ZO-1 localization in MDCK II cells but induced a remarkable increase in ZO-1 gaps in claudins/JAM-A KO cells (Figure 10, A-A', B-B'). As ROCK is well known to regulate actomyosin assembly through myosin activity, I inhibited myosin ATPase activity in MDCK II and claudins/JAM-A KO cells by blebbistatin (Amano M. et al., 1996; Limouze J. et al., 2004). However, blebbistatin had no effect on ZO-1 localization at apical junctions in both two cell lines (Figure 10, C-C'), suggesting that ROCK may act on actomyosin assembly in a myosin-independent pathway.

Previous works established that ROCK can also promote actin assembly by elevating LIM kinase (LIMK) phosphorylation, which in turn inhibitory phosphorylates cofilin, an actin-depolymerizing factor, therefore enhances actin polymerization (Yang et al., 1998; Maekawa et al., 1999). To check, I examined ROCK/ LIMK/ cofilin pathway by treating the cells with LIMK inhibitor BMS-5 (Ross-Macdonald, P. et al., 2008). BMS-5 did not disturb ZO-1 localization at apical junctions in MDCK II cells but strongly enhanced ZO-1 staining discontinuity and ZO-1 gaps in claudins/JAM-A KO cells (Figure 10, D, D'). This suggested that not myosin activity, but actin polymerization indeed plays a crucial role in apical junction integrity of claudins/JAM-A KO cells. To confirm this idea, MDCK II and claudins/JAM-A KO cells were treated with latrunculin A, an actin depolymerizing reagent (Morton et al., 2000). The concentration of

latrunculin A that did not alter ZO-1 continuous staining in MDCK II cells indeed significantly increased ZO-1 gaps observed in claudins/JAM-A KO cells, in a similar manner to LIMK inhibitor treatment (Figure 10, E, E'). Quantification of junction breakage frequency confirmed the drug treatment effects (Figure 10F). Taken together, my data indicate that actin polymerization is critical for the integrity of apical junctions in claudins/JAM-A KO cells.

Both trans-interaction and ZO-1 binding of claudin and JAM-A are required for apical junction integrity

Next, I investigated the molecular mechanism by which claudin and JAM-A maintain apical junction integrity. I hypothesized that claudin and JAM-A may support apical junction integrity in two manners: (1) claudin and JAM-A provide the trans-interactions across cells, most likely to physically tighten and strengthen cell-cell adhesion; (2) claudin and JAM-A provide the membrane anchoring sites for ZO-1 to mechanically couple apical junctions to the actin cytoskeleton.

To clarify these hypotheses, I performed a structure/function analysis of claudin and JAM-A. I designed claudin or JAM-A mutants that were devoid of either trans-interaction or ZO-1 binding activity. For claudin, trans-interaction deficient mutant was generated by substituting amino acid phenylalanine-147th to alanine in claudin-1 (claudin-1[F147A]) (Piontek et al., 2008; Suzuki et al., 2014); ZO-1 binding deficient mutant was created by deleting C-terminal tyrosine-211th and valine-212th to disrupt the PDZ binding motif (claudin-1[ΔYV] (Itoh et al., 2001). For JAM-A, trans-interaction deficient mutant was made by deleting the entire distal loop 1 domain (JAM-A [ΔDL1]) (Monteiro et al., 2014); ZO-1 binding deficient mutant was made by deletion of two C-terminal amino acids leucine-298th and valine-299th to disrupt the PDZ binding motif (JAM-A[ΔLV]) (Itoh et al., 2001). All mutants were validated by stably expressing these mutants in mouse fibroblast L cells and performed co-immunostaining of mutants and ZO-1. In accordance with original studies, both full-length claudin-1 and JAM-A were localized at cell-

cell contacts and recruited ZO-1 (Figure 11, A-A'; B-B'; E-E'; F-F'). Claudin-1[F147A] and JAM-A[ΔDL1] failed to concentrate at cell-cell contacts and did not recruit ZO-1 (Figure 11, C-C'; G-G'). Claudin-1[ΔYV] and JAM-A[ΔLV] were localized at cell-cell contacts but failed to recruit ZO-1 (Figure 11, D-D'; H-H').

Having validated mutant constructs, I established claudins/JAM-A KO cells stably expressing the full-length claudin-1 or JAM-A or their mutants and examined the localization of ZO-1 to evaluate apical junction integrity. A rescue experiment of claudins/JAM-A KO cells expressing full-length claudin-1 fully recovered continuous localization of ZO-1 at apical junctions (Figure 12, A, B). Meanwhile, in claudins/JAM-A KO cells expressing claudin-1[F147A] or claudin-1[ΔYV], ZO-1 still showed discontinuous staining similar to control claudins/JAM-A KO cells (Figure 12, C, D; asterisk). Likewise, full-length JAM-A completely recovered continuous localization of ZO-1 (Figure 12E), whereas neither JAM-A[ΔDL1] nor JAM-A[ΔLV] did not (Figure 12, F-F' arrow, G-G' asterisk). Quantification of junction breakages confirmed the effect of the full-length claudin-1 or JAM-A and their mutants on apical junction integrity in claudins/JAM-A KO cells (Figure 12H). Together, these results indicate that both the trans-interaction and ZO-1 binding of claudin and JAM-A are essential for apical junction integrity.

Claudins and JAM-A are crucial for the conformational change of ZO-1

My findings on the structure-function analysis of claudin and JAM-A suggest a mechanical coupling between neighboring cells mediated by the connection of TJ membrane proteins to the actin cytoskeleton via ZO-1. Recent studies have reported that ZO-1 can carry a mechanical load and undergo conformational change, by which the mechanical force disrupts the intramolecular interaction and extend ZO-1 molecular length (Spararo et al., 2017; Haas et al., 2020). Considering that ZO-1 interacts with claudin, JAM-A and actin cytoskeleton simultaneously via its N-terminal and C-terminal halves, respectively, I hypothesized that claudin and JAM-A

regulate mechanical resistance of apical junctions by regulating the conformational change of ZO-1. To test this, I examined the conformational status of ZO-1 in MDCK II cells and claudins/JAM-A KO cells. The conformational status of ZO-1 in MDCK II cells was investigated in a previous study utilizing molecular fluorescent probing and super-resolution imaging techniques (Spadaro et al., 2017). Based on the original experimental setting, I established claudins/JAM-A KO cells stably expressing exogenous ZO-1 fused with HA-tag and FLAG-tag at its N-terminus and C-terminus, respectively. The conformational status of ZO-1 was examined by measuring the distance between the HA and FLAG tags (Figure 13A). In both MDCK II and claudins/JAM-A KO cells, STED imaging showed that the N-terminus of ZO-1 located at the membrane-proximal regions, while its C-terminus faced the cytoplasm (Figure 13, B, C). Quantitative image analysis of ZO-1 conformational status revealed that 73% of ZO-1 population in MDCK II cells had a distance of more than 60 nm between the N-terminus and C-terminus (Figure 13D), consistent with previous report (Spadaro et al., 2017). In claudins/JAM-A KO cells, the percentage of ZO-1 molecules that had a distance of more than 60 nm between the N-terminus and C-terminus dropped to 53% (Figure 13D). This suggested that ZO-1 molecules in claudins/JAM-A KO cells prefer a “less-stretched” conformation compared to those in MDCK II cells, further suggesting that claudins and JAM-A regulate the conformational change of ZO-1.

CAR is crucial for the nanometer-scale ordering of ZO-1, together with claudin and JAM-A

Despite that the ZO-1 conformation in claudins/JAM-A KO cells was altered compared to MDCK II cells, the orientation of ZO-1 molecules in both cell lines has remained indistinguishable, with the N-terminus of ZO-1 localized at the membrane-proximal regions, while its C-terminus faced to the cytoplasm (Figure 13, B, C). This suggested that other integral membrane proteins may provide the anchoring sites for the N-terminus of ZO-1. I further examined two other TJ-associated integral membrane proteins, occludin and CAR, both of which

interact with ZO-1. To investigate whether occludin or CAR is involved in membrane-proximal localization of the N-terminus of ZO-1, we knock out the gene of occludin or CAR in claudins/JAM-A KO cells to establish claudins/JAM-A/occludin KO cells or claudins/JAM-A/CAR KO cells, respectively. Then, ZO-1 with the N-terminal HA-tag and C-terminal FLAG-tag was transiently expressed in these cells and the spatial orientation of ZO-1 molecules was examined. In claudins/JAM-A/occludin KO cells, the N-terminus of ZO-1 remained at membrane proximal regions, while the C-terminus faced the cytoplasm, similar to what was seen in claudins/JAM-A KO cells (Figure 14, A-A', B-B'). In contrast, the spatial orientation of ZO-1 in claudins/JAM-A/CAR KO cells were relatively more random, by which HA-tag N-terminal ZO-1 could be found at both membrane proximal regions and membrane distal region facing cytoplasm (Figure 14, C-C'). The order parameter was quantified to confirm this random ordering. (Figure 14D). Taken together, my data indicate that CAR, together with claudin and JAM-A, anchor ZO-1 to apical junction proximal regions and are essential for the nanometer-scale ordering of ZO-1.

Claudin, JAM-A, and CAR coordinately regulate apical junction integrity

Finally, I investigated whether CAR is required for the maintenance of apical junction integrity. By immunostaining, I reported that ZO-1 staining was continuous at apical junctions with no junctional breakage detected in the following cells: MDCK II, claudins KO, JAM-A KO, and CAR KO cells, confirmed by quantification of junction breakage phenotype (Figure 14I). Claudins/CAR KO cells exhibited a defect in apical junction integrity with discontinuous localization of ZO-1 along apical junctions, similar to claudins/JAM-A KO cells (Figure 14, E-F). Claudins/JAM-A/occludin KO cells showed a slightly increased junction breakage phenotype compared to claudins/JAM-A KO cells (Figure 14G). In contrast, claudins/JAM-A/CAR KO cells showed severe junction breakage phenotype with various large gaps observed (Figure 14H). Junction breakage frequency in all cell lines was quantified (Figure 14I). Of note, we observed

an increase of CAR levels at apical junctions in claudins/JAM-A KO cells (Figure 15, A, A'), which is further confirmed by the increase of CAR protein expression levels in western blotting assay (Figure 15, B). Altogether, my observations indicate that CAR, in coordination with claudin and JAM-A, is important for the maintenance of apical junction integrity.

Discussion

The roles of TJs in mechanical resistance have remained unclear for a long time. To address this issue, I utilized claudins/JAM-A KO cells, which are epithelial MDCK II cells that lack entire TJ structures and functions, due to the loss of TJ membrane proteins, claudin-1/2/3/4/7 and JAM-A (Otani et al., 2019). My findings indicate that claudin and JAM-A, in coordination with actin cytoskeleton, are essential for apical junction integrity under mechanical stress. My observations suggest that claudin and JAM-A support the apical junction integrity by both providing trans-interactions across cells and membrane anchoring sites for ZO-1, a TJ-specific mechanosensor molecule (Spadaro et al., 2017). Claudin and JAM-A appeared to regulate ZO-1 conformational change, which strongly correlated with the status of apical junction integrity. Strikingly, CAR, another TJ-associated membrane integral protein, collaborates with claudin and JAM-A to support the nanometer-scale ordering of ZO-1 and apical junction integrity. In conclusion, my findings directly demonstrate for the first time that TJ transmembrane proteins, including claudin, JAM-A, and CAR, coordinately regulate apical junction integrity.

The coordinate contribution of TJ transmembrane proteins to the apical junction integrity

It has been widely accepted that claudin contribute to tight junction formation by constituting TJ strand network, while JAM-A and CAR appeared to be involved in multiple cellular signaling pathways (Mandell et al., 2004; Cohen et al., 2001; Ebnet et al.,2022; Excoffon et al., 2004). My results show that claudins/JAM-A KO and claudins/CAR KO cells exhibit focal breakages of apical junctions, while the junction breakage was not observed in MDCK II cells lacking solely claudin, JAM-A, or CAR. These results suggest that TJ transmembrane proteins, including claudin, JAM-A, and CAR coordinately contribute to apical junction integrity.

I reported the elevated CAR levels at apical junctions in claudins/JAM-A KO cells. Two possible explanations are taken into consideration. First, the elimination of claudin and JAM-A may increase the space available at apical junctional regions, leading to an increase in the junctional CAR level. Second, noted that claudins KO cells displayed intact apical junction morphology, and further depletion of either JAM-A or CAR in those cells resulted in an equivalent junction breakage phenotype (Figure 13I). Consider that CAR and JAM-A are members of the TJ-associated immunoglobulin superfamily and share a similar molecular structure (Martin-Padura et al., 1998; Prota AE., 2003), it is possible that the increased production of CAR in claudin/JAM-A KO cells may serve as a defense mechanism against the loss of JAM-A. Overexpression of either CAR in claudins/JAM-A KO cells or JAM-A in claudins/CAR KO cells to test whether it recovers apical junction integrity may help to clarify this second possibility.

My finding showed that regardless of increased CAR levels in claudins/JAM-A KO cells, ZO-1 conformational change was still somewhat altered, with ZO-1 preferring a “less-stretched” conformational status. It raises the question of why elevated CAR levels cannot offset the roles claudin and JAM-A in regulating ZO-1 conformational change. It is possible that CAR may possess a low binding affinity for ZO-1 and cannot hold ZO-1 in place long enough to keep it in the stretched conformation. Another alternative explanation is that CAR contains an SH3-binding domain and may engage with the SH3 domain located at the central region of ZO-1 molecules, making CAR harder to sustain ZO-1 intramolecular stretching. Analyses of the interaction domains and protein binding affinity between CAR and ZO-1 will help to clarify these two scenarios.

The role of ZO-1 conformational change in mechanical resistance

My data revealed that claudins/JAM-A KO cells displayed a “less-stretched” conformation of ZO-1. A previous study has investigated the conformational change of ZO-1 in response to tension, by using single-protein stretching by magnetic tweezers method (Spadaro et al., 2017).

According to that, ZO-1 was designed to have C-terminus firmly attached to the bottom coverslip, while N-terminus fused with paramagnetic beads which were later pulled by a motorized magnet, and the extension of ZO-1 molecule was captured (Spadaro et al., 2017). ZO-1 interacts with TJ membrane proteins at its N-terminal half and with actin cytoskeleton at its C-terminal half, respectively (Itoh et al., 1999; Bazzoni et al., 2000; Ebnet et al., 2000; Itoh et al., 2001; Fanning et al., 1998; Fanning et al., 2002; Belardi et al., 2020). If tensile force is applied between the membrane protein binding sites and the actin-binding site of ZO-1, the ZO-1 molecule could be stretched. One speculation is that the removal of claudin and JAM-A may decrease the N-terminal membrane anchoring sites for ZO-1, leading to ZO-1 molecules resides in "less-stretched" conformation.

In claudins/JAM-A/CAR KO cells, regardless of the lack of membrane anchoring site for ZO-1 provided by claudin, JAM-A, and CAR, ZO-1 was still enriched at apical junctions. It raises the question of what recruits and maintains ZO-1 at the apical junction proximal region under that circumstance. Previous works studying cell-cell junction formation in epithelial cells claimed that ZO-1 was transiently recruited to AJs before translocating to later newly-formed TJs (Rajasekaran et al., 1996; Ando-Akatsuka et al., 1999; Ooshio et al., 2010). In addition, ZO-1 localizes at AJs in non-epithelial cells (Itoh et al., 1991; Itoh et al., 1993; Itoh et al., 1997). Therefore, it is possible that in the loss of TJ membrane proteins, ZO-1 may anchor to AJs via interaction with AJ proteins, e.g., afadin, or a-catenin (Ooshio et al., 2010; Rajasekaran et al., 1996). Another possibility is that ZO-1 may hang on to the circumferential actin network, directly through its actin-binding domain at C-termini, or indirectly through its binding to F-actin-associated proteins, e.g., cingulin (Vasileva et al., 2022). Future investigation to identify the alternative junctional interacting partner of ZO-1 rather than claudin, JAM-A and CAR may help to gain new insight into this issue.

The role of actin polymerization in apical junction integrity

In previous studies, the role of actin cytoskeleton upon junction assembly has been widely accepted (Yonemura et al., 1995; Krendel and Bonder, 1999; Vasioukhin et al., 2000; Verma et al., 2004). Here, my findings indicate that actin polymerization is critical for the apical junction integrity in claudins/JAM-A KO cells. Upon cell stretching, actin disorganization occurred concomitantly with junction breakages, and actin reassembly preceded the relocalization of ZO-1 to apical junctions upon junction repair. It suggests that the actin cytoskeleton may play potential roles in apical junction maintenance and repair, which is consistent with a previous work reported that Rho signaling regulates the repair of small junction breakages via activating actomyosin contractility and actin polymerization (Stephenson et al., 2019). Together, these findings point to the biological importance of actin polymerization in regulating epithelial junction homeostasis.

In conclusion, my study demonstrates that TJ membrane proteins and actin cytoskeleton cooperate to regulate the apical junction integrity against mechanical stress.

References

Amagai, M., V. Klaus-Kovtun, and J.R. Stanley. 1991. Autoantibodies against a novel epithelial cadherin in pemphigus vulgaris, a disease of cell adhesion. *Cell*. 67:869–877.

Amano, M., M. Ito, K. Kimura, Y. Fukata, K. Chihara, T. Nakano, Y. Matsuura, and K. Kaibuchi. 1996. Phosphorylation and Activation of Myosin by Rho-associated. *J. Biol. Chem*. 271:20246–20249.

Anderson, J. M., and C.M. Van Itallie. 2009. Physiology and Function of the Tight Junction. *Cold Spring Harb. Perspect. Biol*. 1:a002584.

Ando-Akatsuka, Y., Saitou, M., Hirase, T., Kishi, M., Sakakibara, A., Itoh, M., Yonemura, S., Furuse, M., & Tsukita, S. 1996. Interspecies diversity of the occludin sequence: cDNA cloning of human, mouse, dog, and rat-kangaroo homologues. *J. Cell Biol.* 133:43–47.

Ando-Akatsuka, Y., S. Yonemura, M. Itoh, M. Furuse, and S. Tsukita. 1999. Differential behavior of E-cadherin and occludin in their colocalization with ZO-1 during the establishment of epithelial cell polarity. *J. Cell. Physiol*. 179:115–125.

Bazzoni, G., O.M. Martínez-Estrada, F. Orsenigo, M. Cordenonsi, S. Citi, and E. Dejana. 2000. Interaction of junctional adhesion molecule with the tight junction components ZO-1, cingulin, and occludin. *J. Biol. Chem*. 275:20520–20526.

Belardi, B., T. Hamkins-Indik, A.R. Harris, J. Kim, K. Xu, and D.A. Fletcher. 2020. A Weak Link with Actin Organizes Tight Junctions to Control Epithelial Permeability. *Dev. Cell*. 54:792–804.

Bergelson, J.M., J.A. Cunningham, G. Droguett, E.A. Kurt-jones, A. Krithivas, J.S. Hong, M.S. Horwitz, R.L. Crowell, and R.W. Finberg. 1997. Isolation of a Common Receptor for Coxsackie B viruses and adenoviruses 2 and 5. *Science.* 275:1320–1323.

Bertocchi, C., Wang, Y., Ravasio, A., Hara, Y., Wu, Y., Sailov, T., Baird, M.A., Davidson, M.W., Zaidel-Bar, R., Toyama, Y., et al. 2017. Nano- scale architecture of cadherin-based cell adhesions. *Nat. Cell Biol*. 19:28–37.

Burridge, K., & Wennerberg, K. 2004. Rho and Rac take center stage. *Cell*. 116:167–179.

Chrzanowska-Wodnicka, M., & Burridge, K. 1996. Rho-stimulated contractility drives the formation of stress fibers and focal adhesions. *J. CellBiol.* 133:1403–1415.

Cohen, C.J., J.T.C. Shieh, R.J. Pickles, T. Okegawa, J.T. Hsieh, and J.M. Bergelson. 2001. The coxsackievirus and adenovirus receptor is a transmembrane component of the tight junction. *Proc. Natl. Acad. Sci. U. S. A.* 98:15191–15196.

Ebnet, K., C.U. Schulz, M.M. Brickwedde, G.G. Pendl, and D. Vestweber. 2000. Junctional Adhesion Molecule Interacts with the PDZ Domain-containing Proteins AF-6 and ZO-1. *J. Biol. Chem*. 275:27979–27988.

Excoffon, K.J.D.A., A. Hruska-Hageman, M. Klotz, G.L. Traver, and J. Zabner. 2004. A role for the PDZ-binding domain of the coxsackie B virus and adenovirus receptor (CAR) in cell adhesion and growth. *J. Cell Sci*. 117:4401–4409.

Fanning, A.S., B.J. Jameson, L.A. Jesaitis, and J.M. Anderson. 1998. The tight junction protein ZO-1 establishes a link between the transmembrane protein occludin and the actin cytoskeleton. *J. Biol. Chem*. 273:29745–29753.

Fanning, A.S., T.Y. Ma, and J.M. Anderson. 2002. Isolation and functional characterization of the actin binding region in the tight junction protein ZO-1. *FASEB J*. 16:1835–1837.

Farquhar, M.G., and G.E. Palade. 1963. Junctional complexes in various epithelia. *J. Cell Biol*. 17:375–412.

Furuse, M., Fujimoto, K., Sato, N., Hirase, T., Tsukita, S., & Tsukita, S. 1996. Overexpression of occludin, a tight junction-associated integral membrane protein, induces the formation of intracellular multilamellar bodies bearing tight junction-like structures. *J. Cell Biol*. 109:429–435.

Furuse, M., K. Fujita, T. Hiiragi, K. Fujimoto, and S. Tsukita. 1998. Claudin-1 and -2: Novel integral membrane proteins localizing at tight junctions with no sequence similarity to occludin. *J. Cell Biol*. 141:1539–1550.

Furuse, M., T. Hirase, M. Itoh, A. Nagafuchi, S. Yonemura, S. Tsukita, and S. Tsukita. 1993. Occludin: A novel integral membrane protein localizing at tight junctions. *J. Cell Biol*. 123:1777–1788.

Furuse, M., M. Itoh, T. Hirase, A. Nagaftichi, S. Yonemura, S. Tsukita, and S. Tsukita. 1994. Direct association of occludin with ZO-1 and its possible involvement in the localization of occludin at tight junctions. *J. Cell Biol*. 127:1617–1626.

Gumbiner, B., T. Lowenkopf, and D. Apatira. 1991. Identification of a 160-kDa polypeptide that binds to the tight junction protein ZO-1. *Proc. Natl. Acad. Sci. U. S. A*. 88:3460–3464.

Günzel, D., and A.S.L. Yu. 2013. Claudins and the modulation of tight junction permeability. *Physiol. Rev*. 93:525–569.

Haas, A.J., C. Zihni, A. Ruppel, C. Hartmann, K. Ebnet, M. Tada, M.S. Balda, and K. Matter. 2020. Interplay between Extracellular Matrix Stiffness and JAM-A Regulates Mechanical Load on ZO-1 and Tight Junction Assembly. *Cell Rep*. 32:107924.

Hall A. (1998). Rho GTPases and the actin cytoskeleton. *Science*. 279:509–514.

Harris, A.R., L. Peter, J. Bellis, B. Baum, A.J. Kabla, and G.T. Charras. 2012. Characterizing the mechanics of cultured cell monolayers. *Proc. Natl. Acad. Sci. U. S. A*. 109:16449–16454.

Higashi, T., T.R. Arnold, R.E. Stephenson, K.M. Dinshaw, and A.L. Miller. 2016. Maintenance of the Epithelial Barrier and Remodeling of Cell-Cell Junctions during Cytokinesis. *Curr. Biol*. 26:1829–1842.

Ishizaki, T., Uehata, M., Tamechika, I., Keel, J., Nonomura, K., Maekawa, M., & Narumiya, S. 2000. Pharmacological properties of Y-27632, a specific inhibitor of rho-associated kinases. *Mol. Pharmacol*. 57:976–983.

Itoh, M., Nagafuchi, A., Yonemura, S., Kitani-Yasuda, T., Tsukita, S., & Tsukita, S. 1993. The 220-kD protein colocalizing with cadherins in non-epithelial cells is identical to ZO-1, a tight junction-associated protein in epithelial cells: cDNA cloning and immunoelectron microscopy. *J. Cell Biol.* 121:491–502.

Itoh, M., M. Furuse, K. Morita, K. Kubota, M. Saitou, and S. Tsukita. 1999. Direct binding of three tight junction-associated MAGUKs, ZO-1, ZO-2, and ZO-3, with the COOH termini of claudins. *J. Cell Biol*. 147:1351–1363.

Itoh, M., A. Nagafuchi, S. Moroi, and S. Tsukita. 1997. Involvement of ZO-1 in cadherin-based cell adhesion through its direct binding to α catenin and actin filaments. *J. Cell Biol*. 138:181–192.

Itoh, M., A. Nagafuchi, S. Yonemura, T. Kitani-Yasuda, S. Tsukita, and S. Tsukita. 1993. The 220-kD protein colocalizing with cadherins in non-epithelial cells is identical to ZO-1, a tight junction-associated protein in epithelial cells: cDNA cloning and immunoelectron microscopy. *J. Cell Biol*. 121:491–502.

Itoh, M., H. Sasaki, M. Furuse, H. Ozaki, T. Kita, and S. Tsukita. 2001. Junctional adhesion molecule (JAM) binds to PAR-3: A possible mechanism for the recruitment of PAR-3 to tight junctions. *J. Cell Biol*. 154:491–497.

Itoh, M., S. Yonemura, A. Nagafuchi, S. Tsukita, and S. Tsukita. 1991. A 220-kD undercoat-constitutive protein: Its specific localization at cadherin-based cell-cell adhesion sites. *J. Cell Biol*. 115:1449–1462.

Kimura, K., M. Ito, M. Amano, K. Chihara, Y. Fukata, M. Nakafuku, B. Yamamori, J. Feng, T. Nakano, K. Okawa, A. Iwamatsu, and K. Kaibuchi. 1996. Regulation of myosin phosphatase by Rho and Rho-associated kinase (Rho-kinase). *Science*. 273:245–248.

Kim, T.J., Zheng, S., Sun, J., Muhamed, I., Wu, J., Lei, L., Kong, X., Leck- band, D.E., and Wang, Y. 2015. Dynamic visualization of alpha-catenin reveals rapid, reversible conformation switching between tension states. *Curr. Biol*. 25:218–224.

Kintner, C. 1992. Regulation of embryonic cell adhesion by the cadherin cytoplasmic domain. *Cell*. 69:225–236.

Kostrewa D, Brockhaus M, D'Arcy A, Dale G. 2001. X-ray structure of junc- tional adhesion molecule: structural basis for homophilic adhesion via a novel dimerization motif. *EMBO J.* 20:4391–4398.

Krendel, M.F., and E.M. Bonder. 1999. Analysis of actin filament bundle dynamics during contact formation in live epithelial cells. Cell Motil. Cytoskeleton. 43:296–309.

Limouze, J., Straight, A. F., Mitchison, T., & Sellers, J. R. 2004. Specificity of blebbistatin, an inhibitor of myosin II. *J. Muscle Res. Cell.* 25:337–341.

Mandai K, Nakanishi H, Satoh A, Obaishi H, Wada M, Nishioka H, Itoh M, Mizoguchi A, Aoki T, Fujimoto T, Matsuda Y, Tsukita S, Takai Y. 1997. Afadin: A novel actin filament-binding protein with one PDZ domain localized at cadherin-based cell-to-cell adherens junction. *J. Cell Biol*. 139(2):517-28.

Mandell, K. J., McCall, I. C., & Parkos, C. A. 2004. Involvement of the junctional adhesion molecule-1 (JAM1) homodimer interface in regulation of epithelial barrier function. *J. Biol. Chem*. 279:16254–16262.

Martìn-Padura, I., S. Lostaglio, M. Schneemann, L. Williams, M. Romano, P. Fruscella, C. Panzeri, A. Stoppacciaro, L. Ruco, A. Villa, D. Simmons, and E. Dejana. 1998. Junctional adhesion molecule, a novel member of the immunoglobulin superfamily that distributes at intercellular junctions and modulates monocyte transmigration. *J. Cell Biol*. 142:117–127.

Maekawa, M., T. Ishizaki, S. Boku, N. Watanabe, A. Fujita, A. Iwamatsu, T. Obinata, K. Ohashi, K. Mizuno, and S. Narumiya. 1999. Signaling from Rho to the actin cytoskeleton through protein kinases ROCK and LIMK-kinase. *Science*. 285:895–898.

Matsunaga, M., K. Hatta, and M. Takeichi. 1988. Role of N-cadherin cell adhesion molecules in the histogenesis of neural retina. *Neuron*. 1:289–295.

McCarthy, K. M., Skare, I. B., Stankewich, M. C., Furuse, M., Tsukita, S., Rogers, R. A., Lynch, R. D., & Schneeberger, E. E. 1996. Occludin is a functional component of the tight junction. *J. Cell Sci*. 109:2287–2298.

Morton, W. M., Ayscough, K. R., & McLaughlin, P. J. 2000. Latrunculin alters the actin-monomer subunit interface to prevent polymerization. *Nat. Cell Biol*. 2:376–378.

Monteiro, A.C., A.C. Luissint, R. Sumagin, C. Lai, F. Vielmuth, M.F. Wolf, O. Laur, K. Reiss, V. Spindler, T. Stehle, T.S. Dermody, A. Nusrat, and C.A. Parkos. 2014. Trans-dimerization of JAM-A regulates Rap2 and is mediated by a domain that is distinct from the cis-dimerization interface. *Mol. Biol. Cell*. 25:1574–1585.

Morita K, Furuse M, Fujimoto K, Tsukita S. 1999. Claudin multigene family encoding four-transmembrane domain protein components of tight junction strands. *Proc. Natl. Acad. Sci. U.S.A*. 96:511–516.

Ooshio, T., R. Kobayashi, W. Ikeda, M. Miyata, Y. Fukumoto, N. Matsuzawa, H. Ogita, and Y. Takai. 2010. Involvement of the interaction of afadin with ZO-1 in the formation of tight junctions in Madin-Darby canine kidney cells. *J. Biol. Chem*. 285:5003–5012.

Otani, T., and M. Furuse. 2020. Tight Junction Structure and Function Revisited. *Trends Cell Biol*. 30:805–817.

Otani, T., T.P. Nguyen, S. Tokuda, K. Sugihara, T. Sugawara, K. Furuse, T. Miura, K. Ebnet, and M. Furuse. 2019. Claudins and JAM-A coordinately regulate tight junction formation and epithelial polarity. *J. Cell Biol*. 218:3372–3396.

Prota AE. 2003. Crystal structure of human junctional adhesion molecule 1: Implications for reovirus binding. *Proc. Natl. Acad. Sci. U. S .A*. 100, 5366–5371.

Rajasekaran, A.K., M. Hojo, T. Huima, and E. Rodriguez-Boulan. 1996. Catenins and zonula occludens-1 form a complex during early stages in the assembly of tight junctions. *J. Cell Biol*. 132:451–463.

Raschperger, E., Thyberg, J., Pettersson, S., Philipson, L., Fuxe, J., & Pettersson, R. F. 2006. The coxsackie- and adenovirus receptor (CAR) is an in vivo marker for epithelial tight junctions, with a potential role in regulating permeability and tissue homeostasis. *Exp. Cell Res*. 312:1566–1580.

Richardson, J.C.W., V. Scalera, and N.L. Simmons. 1981. Identification of two strains of MDCK cells which resemble separate nephron tubule segments. *Biochim. Biophys. Acta*. 673:26–36.

Ridley, A. J., & Hall, A. 1992. The small GTP-binding protein rho regulates the assembly of focal adhesions and actin stress fibers in response to growth factors. *Cell*. 70:389–399.

Ross-Macdonald, P., de Silva, H., Guo, Q., Xiao, H., Hung, C. Y., Penhallow, B., Markwalder, J., He, L., Attar, R. M., Lin, T. A., Seitz, S., Tilford, C., Wardwell-Swanson, J., & Jackson, D. 2008. Identification of a nonkinase target mediating cytotoxicity of novel kinase inhibitors. *Mol. Cancer Ther*. 7:3490–3498.

Saito, A. C., Higashi, T., Fukazawa, Y., Otani, T., Tauchi, M., Higashi, A. Y., Furuse, M., & Chiba, H. 2021. Occludin and tricellulin facilitate formation of anastomosing tight-junction strand network to improve barrier function. *Mol. Biol. Cell*. 32:722–738.

Saitou, M., Y. Ando-Akatsuka, M. Itoh, M. Furuse, J. Inazawa, K. Fujimoto, and S. Tsukita. 1997. Mammalian occludin in epithelial cells: its expression and subcellular distribution. *Eur. J. Cell Biol*. 73:22–231.

Sakakibara, A., Furuse, M., Saitou, M., Ando-Akatsuka, Y., & Tsukita, S. (1997). Possible involvement of phosphorylation of occludin in tight junction formation. *J. Cell Biol*. 137:1393–1401.

Shen, L., C.R. Weber, D.R. Raleigh, D. Yu, and J.R. Turner. 2011. Tight Junction Pore and Leak Pathways: A Dynamic Duo. *Annu. Rev. Physiol*. 73:283–309.

Shirayoshi, Y., A. Nose, K. Iwasaki, and M. Takeichi. 1986. N-linked oligosaccharides are not involved in the function of a cell-cell binding glycoprotein E-cadherin. *Cell Struct. Funct*. 11:245–252.

Spadaro, D., S. Le, T. Laroche, I. Mean, L. Jond, J. Yan, and S. Citi. 2017. Tension-Dependent Stretching Activates ZO-1 to Control the Junctional Localization of Its Interactors. *Curr. Biol*. 27:3783–3795.

Staehelin LA. 1974. Structure and function of intercellular junctions. *Int. Rev. Cytol*. 39:191–283.

Stephenson, R.E., T. Higashi, I.S. Erofeev, T.R. Arnold, M. Leda, A.B. Goryachev, and A.L. Miller. 2019. Rho Flares Repair Local Tight Junction Leaks. *Dev. Cell*. 48:445–459.

Stevenson, B.R., J.D. Siliciano, M.S. Mooseker, and D.A. Goodenough. 1986. Identification of ZO-1: A high molecular weight polypeptide associated with the tight junction (Zonula Occludens) in a variety of epithelia. *J. Cell Biol*. 103:755–766.

Suzuki, H., T. Nishizawa, K. Tani, Y. Yamazaki, A. Tamura, R. Ishitani, N. Dohmae, S. Tsukita, O. Nureki, and Y. Fujiyoshi. 2014. Crystal structure of a claudin provides insight into the architecture of tight junctions. *Science*. 344:304–307.

Takeichi, M. 1991. Cadherin cell adhesion receptors as a morphogenetic regulator. *Science*. 251:1451–1455.

Tash, B. R., Bewley, M. C., Russo, M., Keil, J. M., Griffin, K. A., Sundstrom, J. M., Antonetti, D. A., Tian, F., & Flanagan, J. M. 2012. The occludin and ZO-1 complex, defined by small angle X-ray scattering and NMR, has implications for modulating tight junction permeability. *Proc. Natl. Acad. Sci. U. S. A*. 109:10855–10860.

Thölmann, S., Seebach, J., Otani, T., Florin, L., Schnittler, H., Gerke, V., Furuse, M., & Ebnet, K. 2022. JAM-A interacts with α3β1 integrin and tetraspanins CD151 and CD9 to regulate collective cell migration of polarized epithelial cells. CMLS, 79(2), 88.

Umeda, K., J. Ikenouchi, S. Katahira-Tayama, K. Furuse, H. Sasaki, M. Nakayama, T. Matsui, S. Tsukita, M. Furuse, and S. Tsukita. 2006. ZO-1 and ZO-2 Independently Determine Where Claudins Are Polymerized in Tight-Junction Strand Formation. *Cell*. 126:741–754.

Vasileva, E., D. Spadaro, F. Rouaud, J.M. King, A. Flinois, J. Shah, S. Sluysmans, I. Méan, L. Jond, J.R. Turner, and S. Citi. 2022. Cingulin binds to the ZU5 domain of scaffolding protein ZO-1 to promote its extended conformation, stabilization, and tight junction accumulation. *J. Biol. Chem*. 298:101797.

Vasioukhin, V., C. Bauer, M. Yin, and E. Fuchs. 2000. Directed Actin Polymerization is the Driving Force for Epithelial Cell-Cell Adhesion. Cell. 100:209–219.

Verma, S., A.M. Shewan, J.A. Scott, F.M. Helwani, N.R. Den Elzen, H. Mikill, T. Takenawa, and A.S. Yap. 2004. Arp2/3 activity is necessary for efficient formation of E-cadherin adhesive contacts. J. Biol. Chem. 279:34062–34070.

Yang, N., O. Higuchi, K. Ohashi, K. Nagata, A. Wada, K. Kangawa, E. Nishida, and K. Mizuno. 1998. Cofilin phosphorylation by LIM-kinase 1 and its role in Rac-mediated actin reorganization. *Nature*. 393:809–812.

Yonemura, S., M. Itoh, A. Nagafuchi, and S. Tsukita. 1995. Cell-to-cell adherens junction formation and actin filament organization: similarities and differences between non-polarized fibroblasts and polarized epithelial cells. J. Cell Sci. 108:127–142.

Yonemura, S., Y. Wada, T. Watanabe, A. Nagafuchi, and M. Shibata. 2010. α-Catenin as a tension transducer that induces adherens junction development. *Nat. Cell Biol*. 12:533–542.

Zihni, C., C. Mills, K. Matter, and M.S. Balda. 2016. Tight junctions: From simple barriers to multifunctional molecular gates. *Nat. Rev. Mol. Cell Biol*. 17:564–580.

Figures

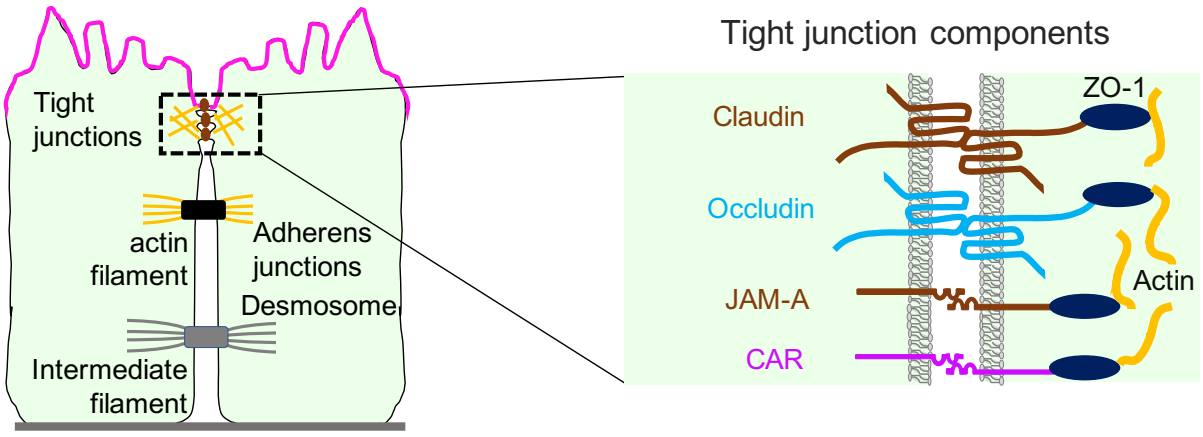

Figure 1. Molecular structure of tight junctions

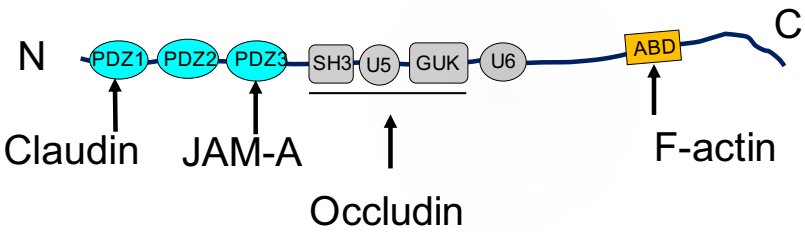

Figure 2. Molecular structure of ZO-1 and its interacting partners

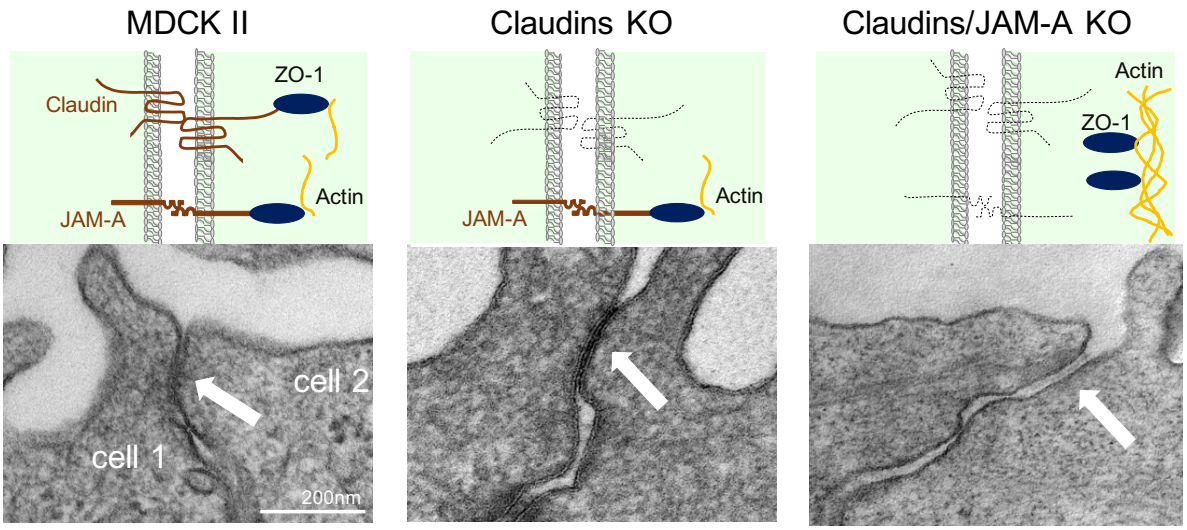

Figure 3. Establishment of claudins/JAM-A KO cells, which completely and specifically lack TJ structure and function

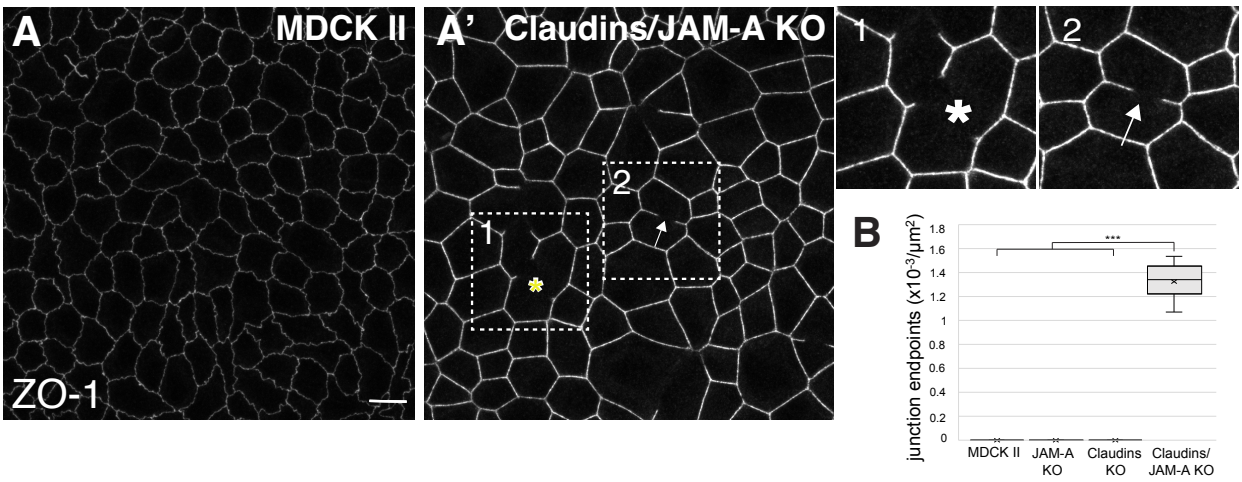

Figure 4. Definition of junction breakage phenotype in claudins/JAM-A KO cells

(**A**) ZO-1 staining of MDCK II cells. ZO-1 staining was continuous along apical junctions.

(**A'**) ZO-1 staining of claudins/JAM-A KO cells. Erratic discontinuity of ZO-1 staining was observed (arrow) or large gap (asterisk).

(**A"**) Quantification of junction breakage frequency. Graphs show endpoint counts of ZO-1 staining per μm^2; data represent mean ± SD (n=9); ***p<0.0005, compared by one-way ANOVA followed by Tukey's test. Scale bars 10μm.

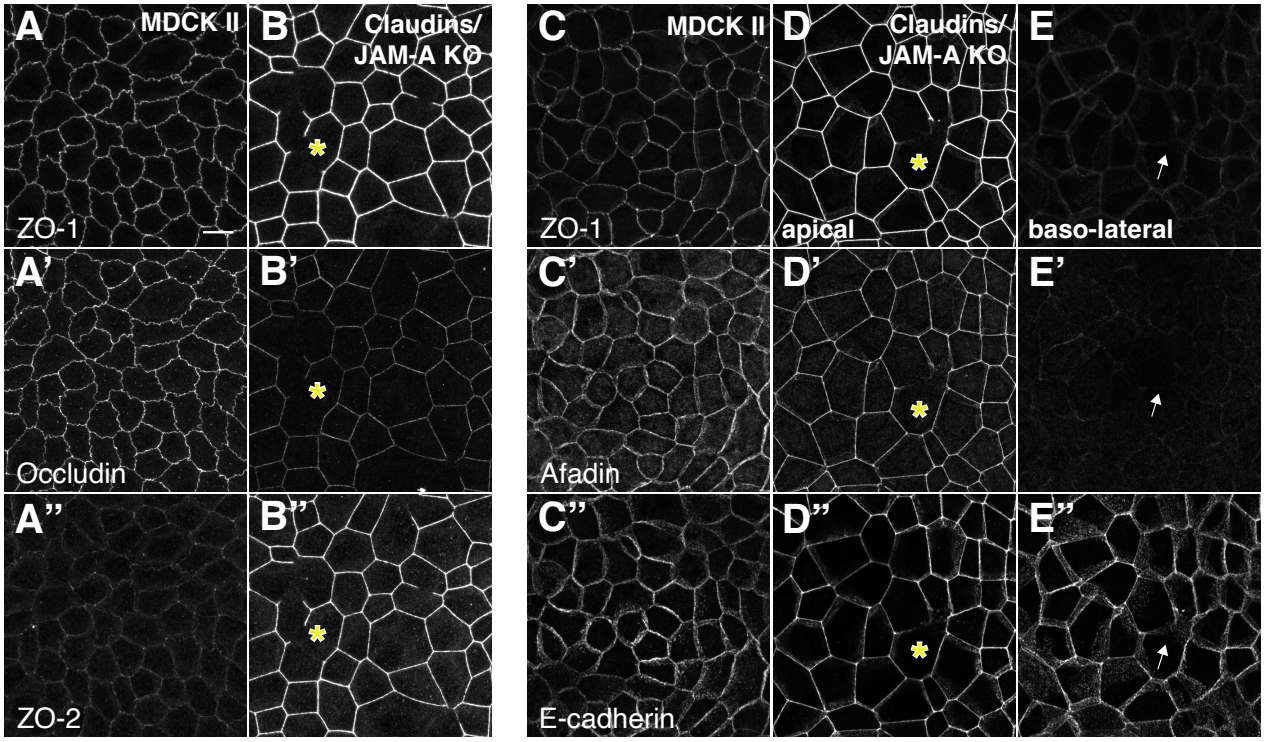

Figure 5. Apical junctions were compromised in claudins/JAM-A KO cells

(**A-B"**) Triple immunostaining of ZO-1, Occludin, and ZO-2 in MDCK II cells (A-A") and claudins/JAM-A KO cells (B-B")

(**C-E"**) Triple immunostaining of ZO-1, Afadin, and E-cadherin in MDCK II cells (C-C") and claudins/JAM-A KO cells (D-D":apical view/ E-E": lateral view). Scale bar 10μm.

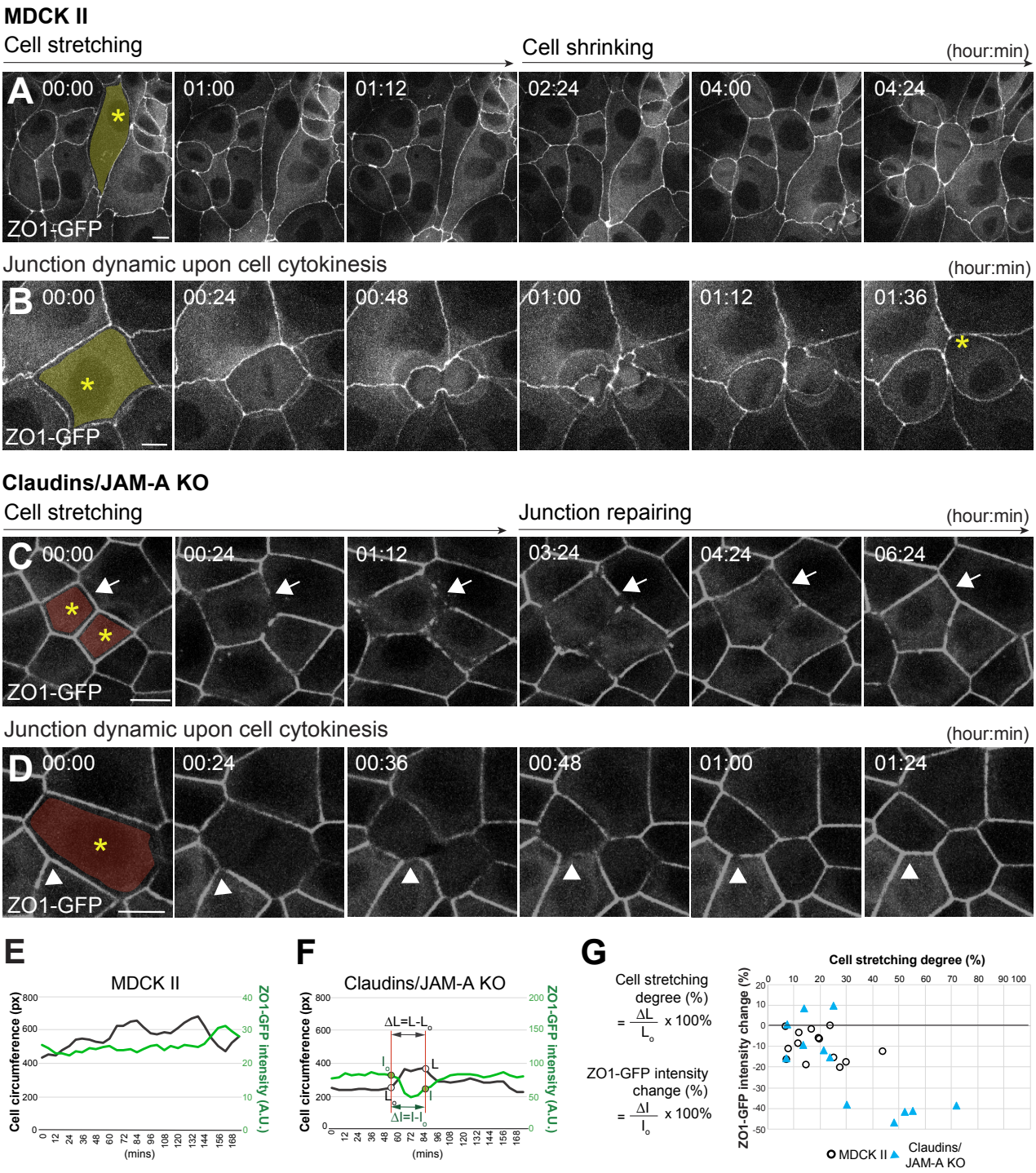

Figure 6. Cell stretching provokes junction breakages

(**A, B**) Snapshots of time-lapse movie of junction dynamic in MDCK II cells expressing ZO1-GFP upon cell stretching (A) and cytokinesis (B). In all cases ZO-1 signal maintained detectable along apical junctions, indicates intact junctions.

(**C, D**) Snapshots of time-lapse movie depicting junction dynamic in claudins/ JAM-A KO cells expressing ZO1-GFP. Junction breakage was captured upon cell stretching (C; arrow) and cytokinesis (D; arrowhead).

(**E, F**) Quantification of the change in the cell circumference (black), and ZO-1 intensity (green) upon cell stretching event of MDCK II cells shown in A (E) and claudins/JAM-A KO cells shown in C (F).

(**G**) Scatter plot showing relationship between cell stretching degree (%) and ZO-1 intensity change (%) in multiple cell-stretching events in MDCK II (black circle) and claudins/JAM-A KO (blue triangle) cells.

Scale bars: 10 μm.

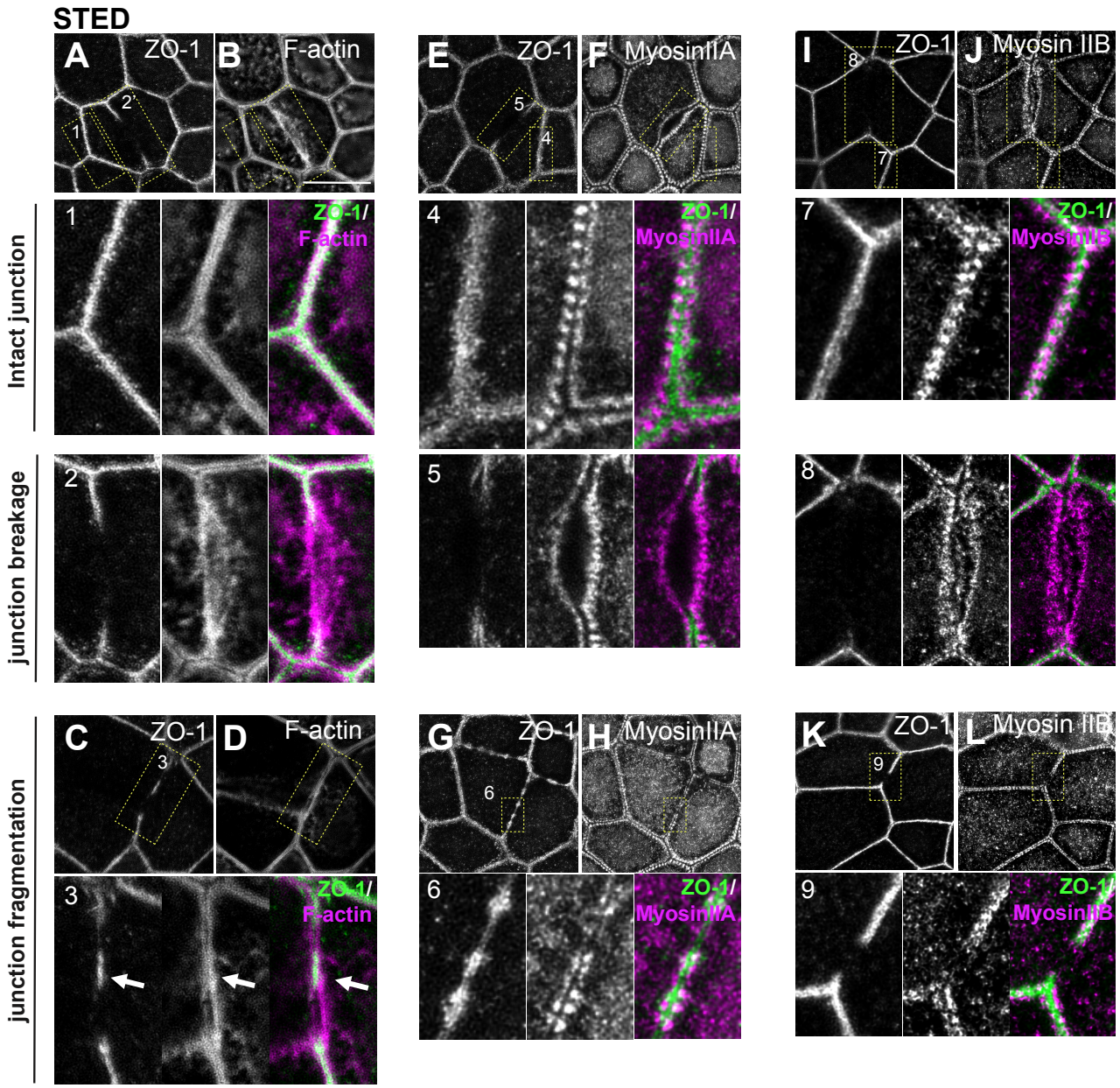

Figure 7. Actomyosin disorganization at junction breakage sites

(**A-D**) STED imaging analysis of F-actin localization at intact junction (A,B-1), large gap (A,B-2) and junction fragmentation (C,D-3). Noted that F-actin again incorporated into junctional area where ZO-1 junctional localization remained (white arrow).

(**E-H**) STED imaging analysis of Myosin IIA localization.

(**I-L**) STED imaging analysis of Myosin IIB localization.

Scale bars: 10 μm.

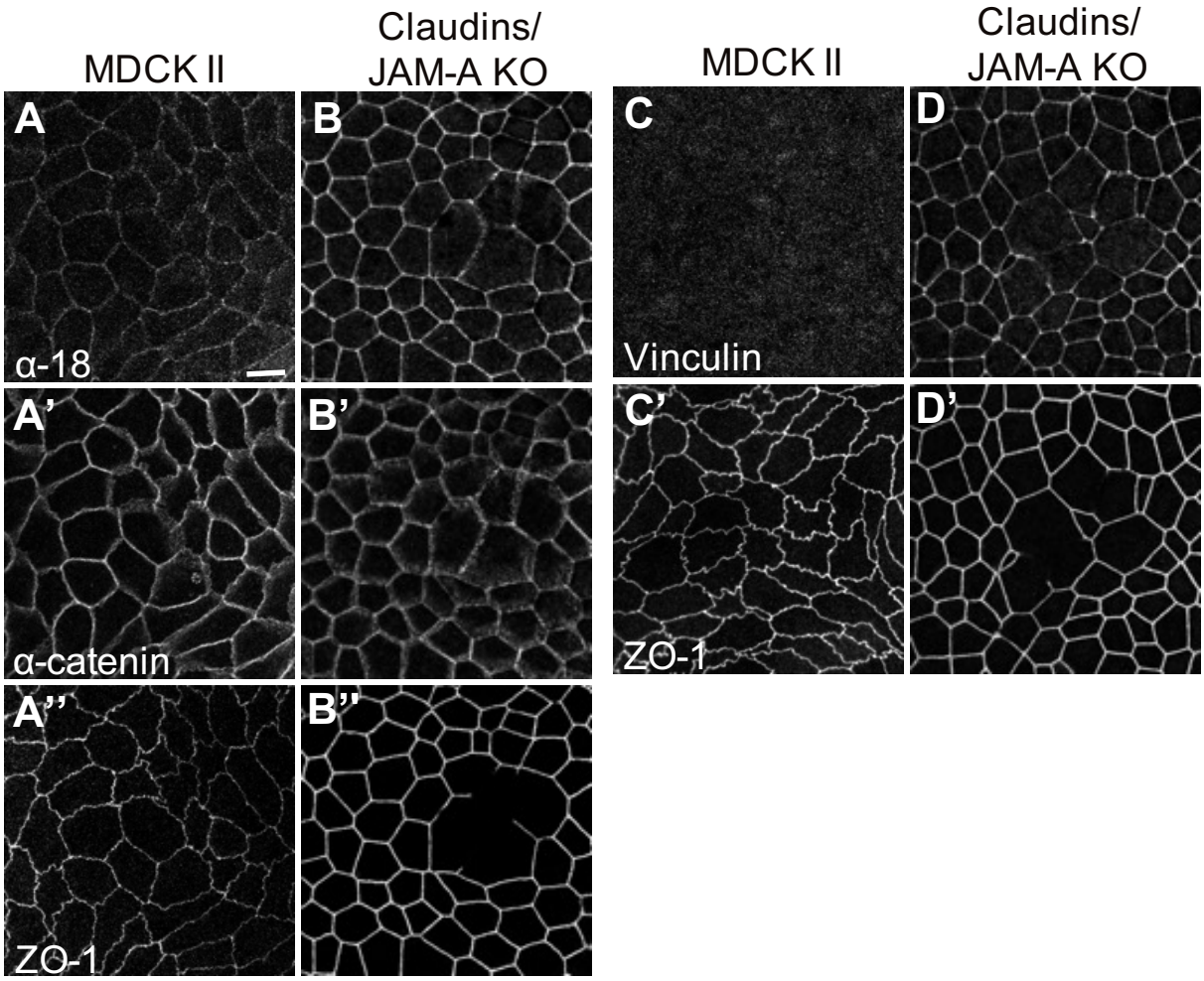

Figure 8. Intercellular tension is elevated along apical junctions in claudins/JAM-A KO cells

(**A-A"**) α-18/α-catenin/ZO-1 triple staining in MDCK II cells. The α-18 antibody recognizes a cryptic epitope exposed by the tension-dependent stretching of α-catenin. Weak staining of α-18 along the apical cell junctions was observed.

(**B-B"**) α-18/α-catenin/ZO-1 triple staining in claudins/JAM-A KO cells. Strong staining of α-18 was observed at the apical junctions, while weak staining was present at the junction breakage sites.

(**C-C'**) Vinculin/ZO-1 double staining in MDCK II cells. Junctional staining was hardly visible in confluent monolayers.

(**D-D'**) Vinculin/ZO-1 double staining in claudins/JAM-A KO cells. Strong accumulation of vinculin was observed at the apical junctions, while weak staining was noted at the junction breakage sites.

Scale bar: 10 μm.

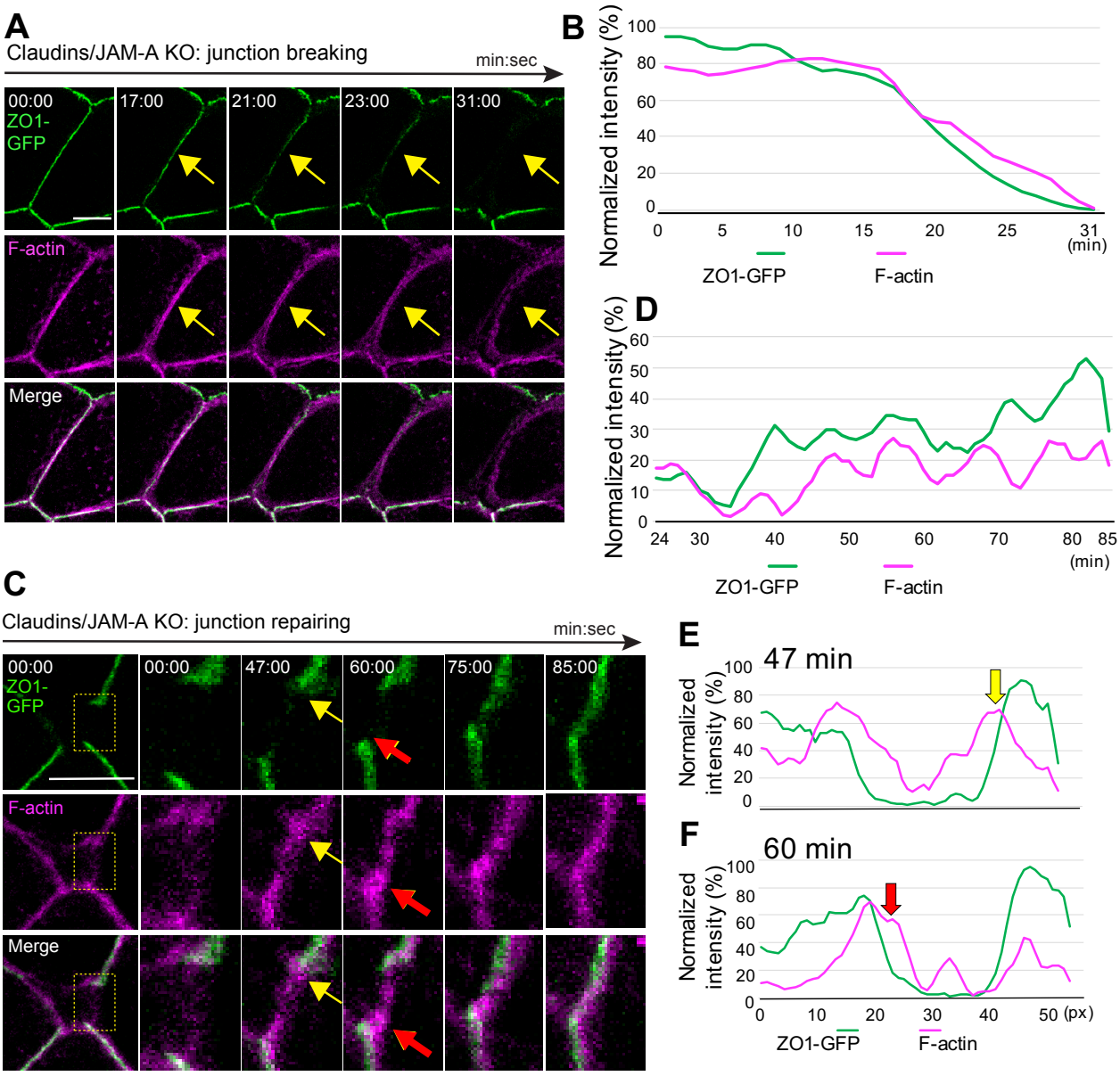

Figure 9. Live-imaging reveals spatial-temporal coupling between F-actin disorganization and junction breakages

(**A,C**) Snapshots of a two-color time-lapse movie in claudins/JAM-A KO cells expressing ZO1-GFP (green) and Lifeact7-mCherry (magenta), depicting a junction breakage event (A; yellow arrow indicate junction breakage) and junction repair event (C).

(**B,D**) Quantification of the junctional fluorescent intensity upon junction breakage shown in A (B) and junction repair shown in C (D).

(**E, F**) Line scan along the junction shown in C at 47 min (E) and 60 min (F). Reassembly of the cell junction-associated actin bundles preceded the recovery of ZO1-GFP to junctions (yellow dotted box: zoom; yellow and red arrows indicate that F-actin accumulation precede ZO-1 relocalization to junctions). Scale bars: 10 μm.

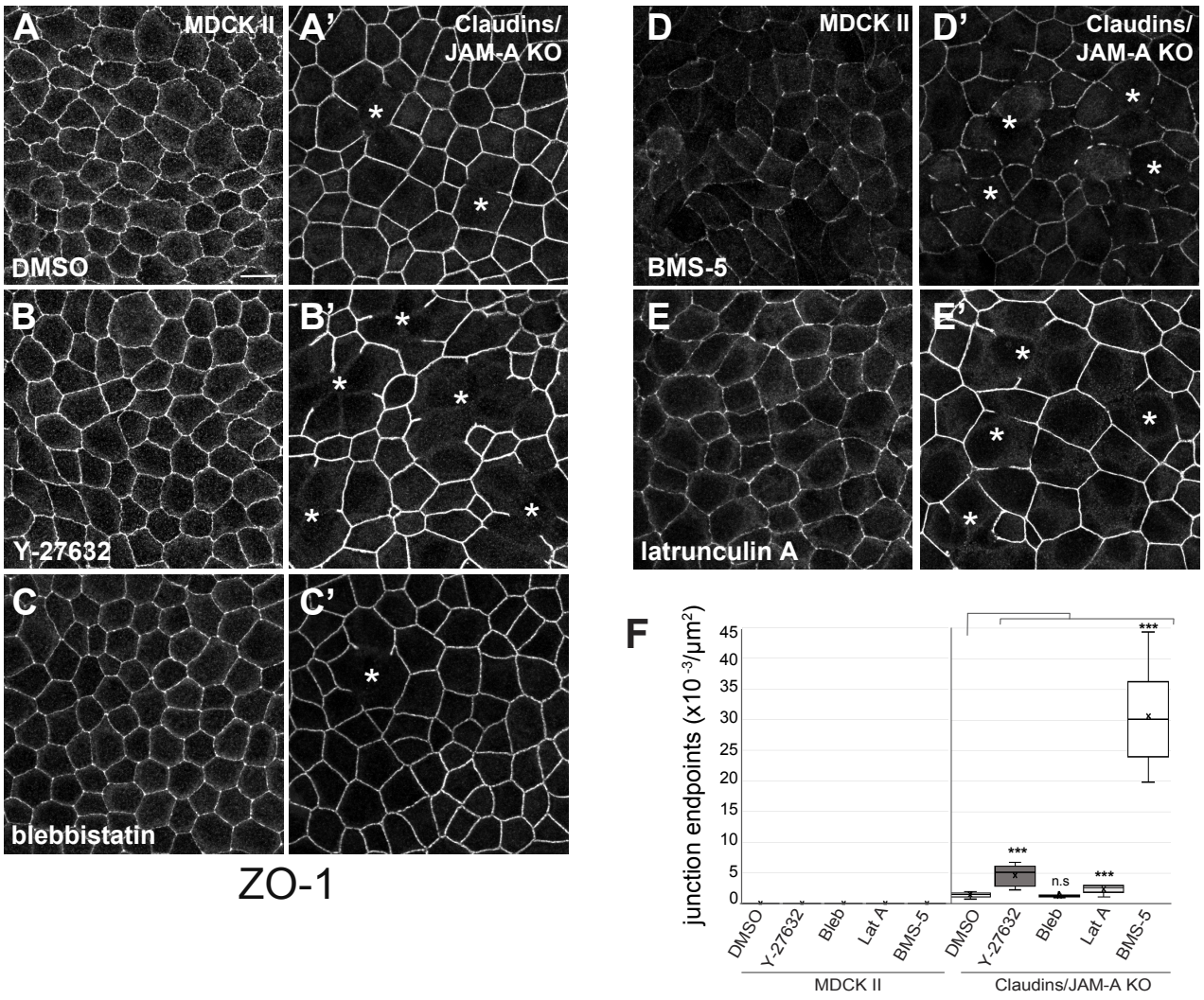

Figure 10. Actin polymerization is critical for apical junction integrity in claudins/JAM-A KO cells

(**A, A'**) ZO-1 staining in DMSO treatment. (A) MDCK II cells; (A') claudins/JAM-A KO cells.

(**B, B'**) ZO-1 staining of ROCK inhibitor Y-27632 treatment (10µM, 3h). (B) MDCK II cells;(B') claudins/JAM-A KO cells.

(**C, C'**) ZO-1 staining of Myosin ATPase activity inhibitor blebbistatin treatment (100µM, 3h). (C) MDCK II cells; (C') claudins/JAM-A KO cells.

(**D, D'**) ZO-1 staining of LIMK inhibitor BMS-5 treatment (10µM, 3h). (C) MDCK II cells; (C') claudins/JAM-A KO cells.

(**E, E'**) ZO-1 staining of action depolymerizing reagent latrunculin A treatment (0.3 µM, 1h). (C) MDCK II cells; (C') claudins/JAM-A KO cells.

(**F**) Quantification of junction breakage frequency. Graphs show endpoint counts of ZO-1 staining per μm^2; data represent mean ± SD (n=9); ***p<0.0005, n.s: non significant, compared by one-way ANOVA followed by Tukey's test. Scale bars: 10µm

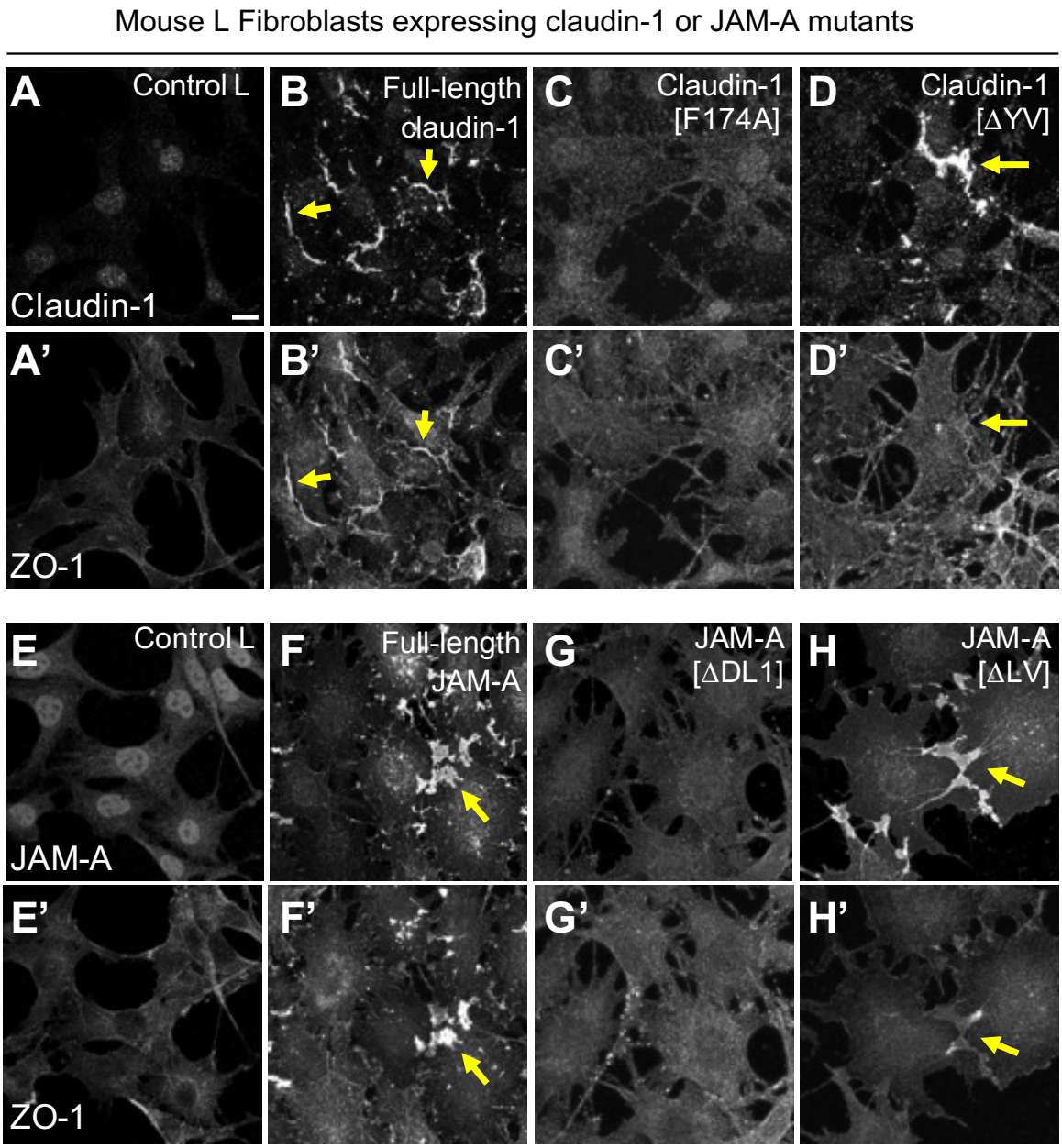

Figure 11. Validation of claudin and JAM-A mutants in mouse fibroblast cells (L cells)

(**A-D'**) Validation of claudin-1 mutants by co-immunostaining claudin-1 (A, B, C, D) and ZO-1 (A', B', C', D'). Control L cells (A-A'); L cells express full-length claudin-1 showed claudin-1 enriches at cell-cell contacts and recruits ZO-1 (B-B', arrow); L cells express trans-interaction deficient mutant claudin-1[F147A] show no claudin-1 and ZO-1 accumulation at cell-cell contacts (C-C', arrow); L cells express ZO-1 binding deficient mutant claudin-1[ΔYV] showed claudin-1 enriches at cell-cell contacts and do not recruit ZO-1 (D-D'; arrow). (**E-H'**) Validation of JAM-A mutants by co-immunostaining JAM-A (E, F, G, H) and ZO-1 (E', F', G', H'). Control L cells (E-E'); L cells express full length JAM-A showed JAM-A enriches at cell-cell contacts and recruits ZO-1 (F-F', arrow); L cells express trans-interaction deficient mutant JAM-A[ΔDL1] show no JAM-A and ZO-1 staining at cell-cell contacts (G-G', arrow); L cells express ZO-1 binding deficient mutant JAM-A[ΔLV] showed JAM-A enriches at cell-cell contacts but not recruit ZO-1 (H-H'; arrow). Scale bar: 10 μm.

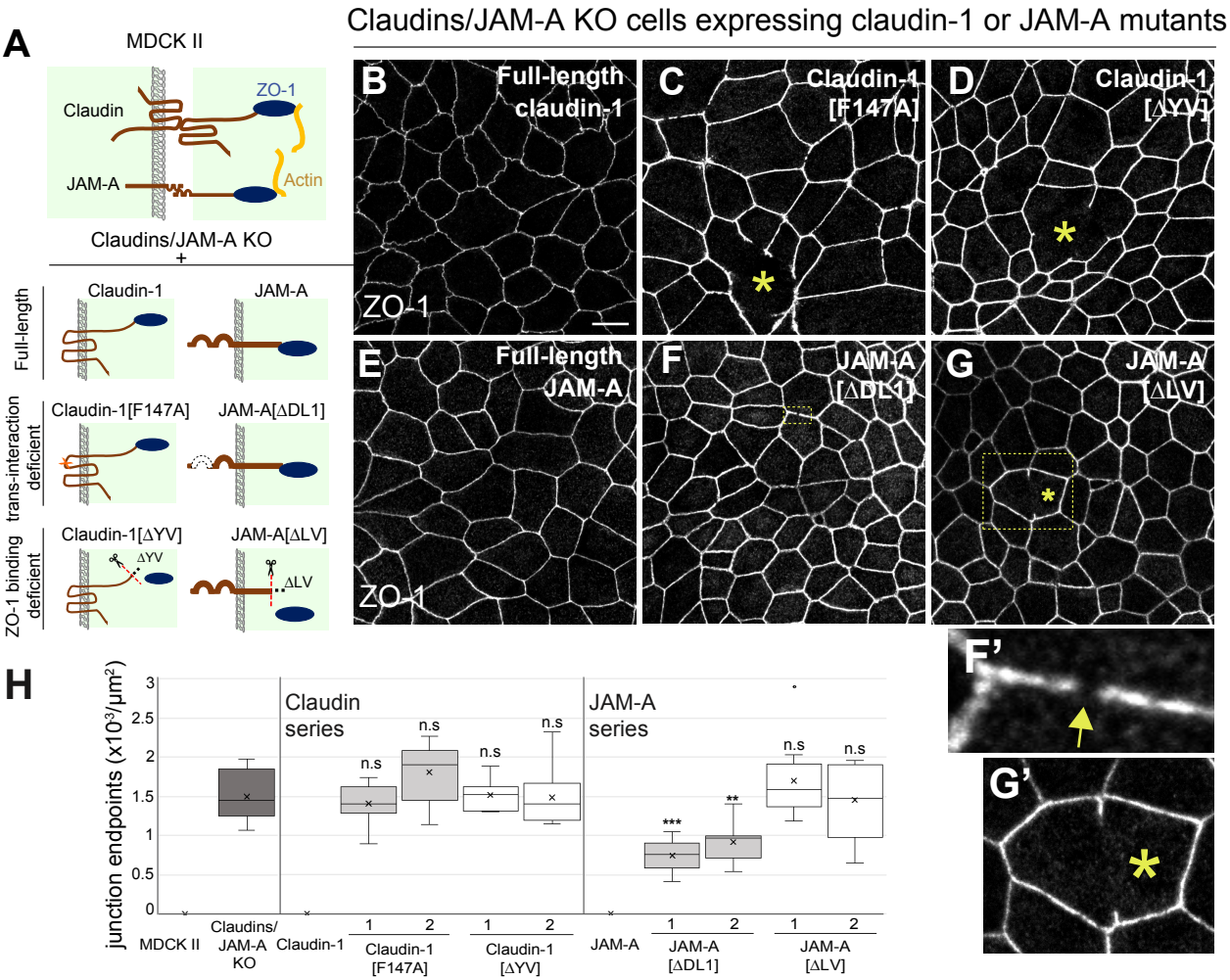

Figure 12. Both the trans-interaction and ZO-1 binding of claudin and JAM-A are required to maintain apical junction integrity.

(**A**) Diagram of the constructs used in this study.

(**B-D**) ZO-1 staining of claudins/JAM-A KO cells expressing full-length claudin-1 (B), claudin-1[F147A] (C), or claudin-1[ΔYV].

(**E-G**) ZO-1 staining of claudins/JAM-A KO cells expressing full-length JAM-A (E), JAM-A[ΔDL1] (F), or JAM-A[ΔLV].

(**H**) Quantification of the junction breakage frequency. Graph displays the endpoint counts of ZO-1 staining per unit area and are presented as mean ± SD (n=9). ***p<0.0005, **p<0.005, n.s: non-significant, compared by one-way ANOVA followed by Tukey's test. Scale bars: 10 μm.

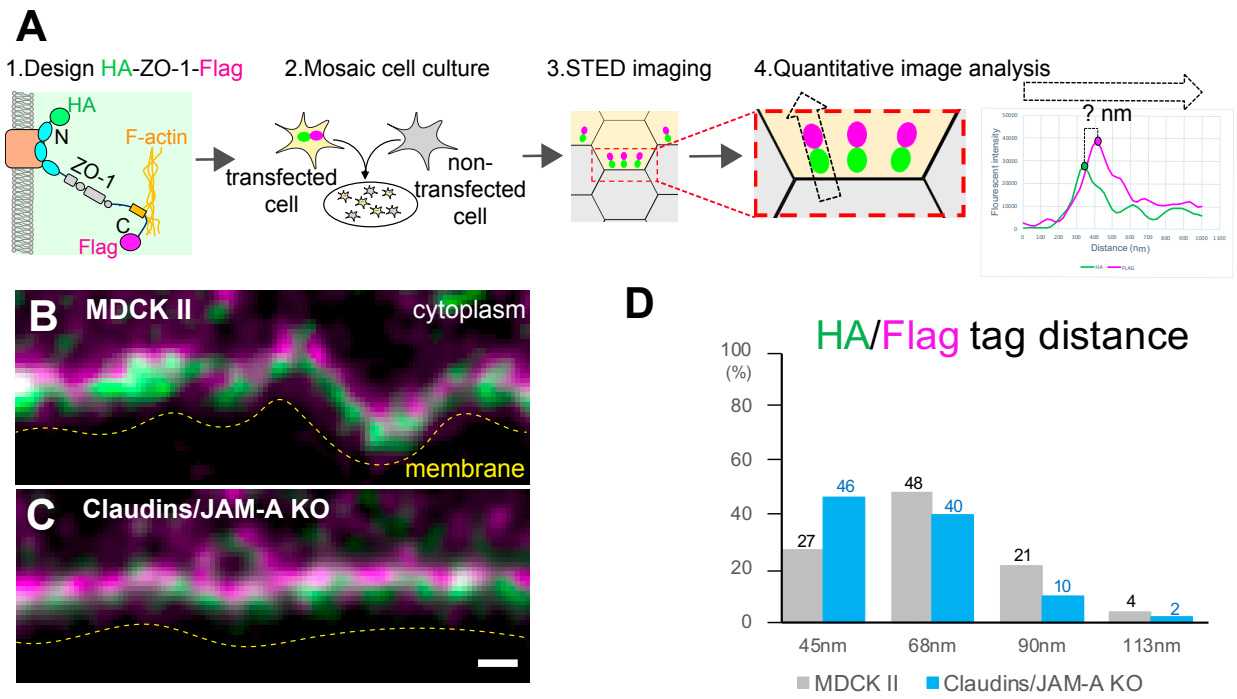

Figure 13. Claudins and JAM-A regulate conformational change of ZO-1

(**A**) Schematic illustration of experimental design.

(**B,C**) STED imaging of HA-ZO1-FLAG to visualize ZO-1 N-terminal HA-tag (green) and a C-terminal FLAG-tag (magenta) in (B) MDCK II cells; (C) claudins/JAM-A KO cells.

(**D**) Distribution of ZO-1 conformation status in MDCK II and claudins/JAM-A KO cells: quantitative analysis of distance between the ZO-1 N-terminal HA-tag (green) and its C-terminal FLAG-tag (magenta). Number of percentages of ZO-1 population with different molecular stretching levels (45/68/90/113 nm) were indicated above each column; (n=100 particles from 10 different junctions in each cell lines). Scale bars: 200 nm.

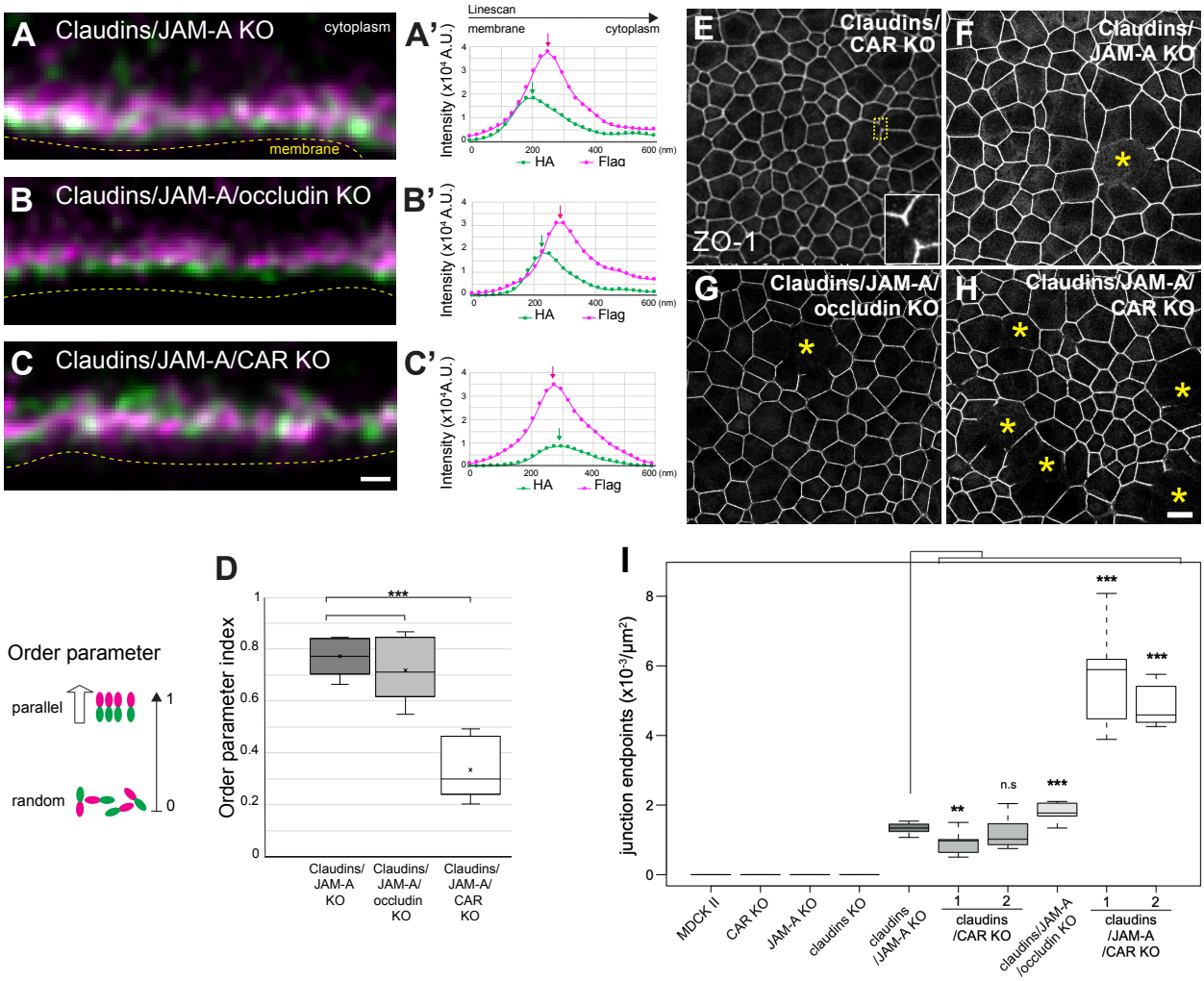

Figure 14. Further removal of CAR from claudins/JAM-A KO cells disrupts membrane-proximal localization of ZO-1 N-terminus, accompanied with severe junction breakages

(**A-C**) STED imaging of ZO-1 N-terminal HA-tag (green) and a C-terminal FLAG-tag (magenta) in (A) claudins/JAM-A KO cells; (B) claudins/JAM-A/occludin KO cells; (C) claudins/JAM-A/CAR KO cells.

(**A'-C'**) Thick linescan cross the membrane shown in A, B, and C; respectively.

(**D**) Quantification of order parameter of ZO-1 in three cell lines show no remarkable difference between claudins/JAM-A KO and claudins/JAM-A/occludin KO cells. Claudins/JAM-A/CAR KO cells display smaller S value indicating a more random ZO-1 nanometer-scale ordering.

(**E-H**) ZO-1 staining in claudins/CAR KO (E), claudins/JAM-A KO (F), claudins/JAM-A/occludin KO (G), and claudins/JAM-A/CAR KO cells (H). Yellow dotted box indicated zoom images; asterisk: ZO-1 gap

(**I**) Quantification of the junction breakage frequency. Graphs showed endpoints counts of ZO-1 staining per μm^2 and are presented as mean ± SD (n=9). ***p<0.0005, **p<0.005, n.s: non-significant; compared by one-way ANOVA followed by Tukey's test. Scale bars: (A-C) 200nm; (E-H) 10μm.

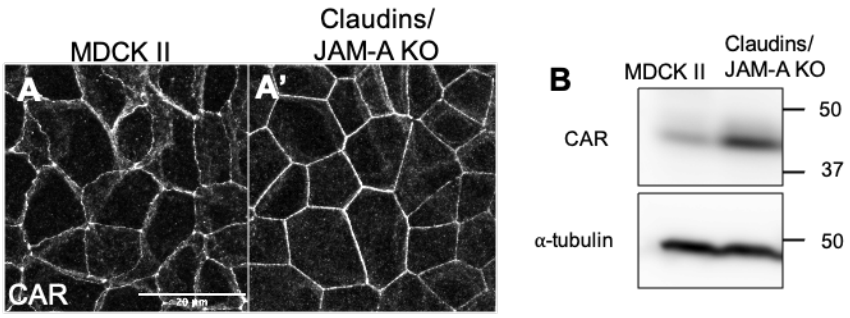

Figure 15. Elevated CAR levels observed in claudins/JAM-A KO cells

(**A-A'**) CAR immuno-staining in MDCK II and claudins/JAM-A KO cells.

(**B**) Western blotting of CAR expression levels in MDCK II and claudins/JAM-A KO cells. Control α-tubulin. Scalebar 20 μm.

Acknowledgments

I would like to express my sincere gratitude to my supervisor, Dr. Mikio Furuse, and my mentor, Dr. Tetsuhisa Otani, for their invaluable guidance and assistance throughout my research. I am beyond grateful for how you patiently walked me through each step of my Ph.D. journey, from being a beginner to becoming a competent scientist, while in the meantime respectfully treating me like one. Thank you so much for your unwavering support during the many ups and downs of both my Ph.D. research and daily life.

I would like to thank my out-of-lab mentors, Dr. Yoshihiro Kubo and Dr. Masumi Hirabayashi, for their invaluable comments and suggestions on my research. I also thank Dr. Akira Nagafuchi (Nara Medical University) for the kind gift of α-18 monoclonal antibody; Dr. Jeffrey M. Bergelson for the kind gift of CAR antibody; Dr. Toshihiko Fujimori (National Institute for Basic Biology) and ABiS (Advanced Bioimaging Support) for the assistance of time-lapse imaging; Dr. Motosuke Tsutsumi and Dr. Tomomi Nemoto for the assistance of STED imaging; Dr. Sachiko Fujiwara for providing research materials and experimental guidance; Mrs. Mika Watanabe and Dr. Yuichiro Kano for technical assistance; and all members in Furuse laboratory for discussion and comments.

I would like to acknowledge the research funding provided by Encouraging Grant for NIPS Graduate Students (AY2020 and AY 2021), the SOKENDAI student dispatch program (AY2022; SDP223108); and the Japanese Government (MEXT) scholarship (AY2018-2023).

Lastly, I am thankful for my best friends, May, Gap, Cici, Lee, Long, Hoa, and Bich, for their mental support and encouragement during my Ph.D. And my family, the best resource through it all – my parent and my younger brother, sincerely thank for their unconditional love, and always being the strongest mental backup of my life.